Eur. Phys. J. Spec. Top. (2026) 235:1469–1491
https://doi.org/10.1140/epjs/s11734-025-01803-9

THE EUROPEAN PHYSICAL JOURNAL SPECIAL TOPICS

Review

Relativistic quantum invariance of QED and QCD

Chueng-Ryong Ji[a]

Department of Physics, North Carolina State University, Box 8202, Raleigh, NC 27695, USA

Received 16 February 2025 / Accepted 8 July 2025 / Published online 22 July 2025

Abstract Relativistic quantum invariance plays prominent roles in the study of quantum field theories, typically QED and QCD. We utilize the idea of interpolating the instant form dynamics (IFD) and the light-front dynamics (LFD) to realize the relativistic quantum invariance of QED and QCD. Reviewing the connection between LFD and IFD using the idea of interpolating the two different forms of the relativistic dynamics, one can learn the distinguished features of each form and how one may utilize those distinguished features in solving the complicated relativistic quantum field theoretic problems more effectively. This review aims at presenting the basic first-hand knowledge of connecting the IFD and the LFD using the idea of interpolation, and demonstrating explicit examples of its utility in QED and QCD.

1 Introduction

For the study of relativistic particle systems, Dirac [1] proposed three different forms of the relativistic Hamiltonian dynamics in 1949: i.e. the instant ($x^0 = 0$), front ($x^+ = (x^0 + x^3)/\sqrt{2} = 0$), and point ($x_\mu x^\mu = a^2 > 0$, $x^0 > 0$) forms. The instant form dynamics (IFD) of quantum field theories is based on the usual equal time $t = x^0$ quantization (units such that $c = 1$ are taken here), which provides a traditional approach evolved from the non-relativistic dynamics. The IFD makes a close contact with the Euclidean space, developing temperature-dependent quantum field theory, lattice QCD, etc. The equal light-front time $\tau \equiv (t + z/c)/\sqrt{2} = x^+$ quantization yields the front form dynamics, nowadays more commonly called light-front dynamics (LFD), which provides an innovative approach to the study of relativistic dynamics. The LFD works strictly in the Minkowski space, developing useful frameworks for the analyses of deep inelastic scattering (DIS), parton distribution functions (PDFs), deeply virtual Compton scattering (DVCS), generalized parton distributions (GPDs), etc. The quantization in the point form ($x^\mu x_\mu = a^2 > 0$, $x^0 > 0$) is called radial quantization and this quantization procedure has been much used in string theory and conformal field theories [2] as well as in hadron physics [3–5]. Among these three forms of relativistic dynamics proposed by Dirac, however, the LFD carries the largest number (seven) of the kinematic (or interaction independent) generators leaving the least number (three) of the dynamics generators, while both the IFD and the point form dynamics carry six kinematic and four dynamic generators within the total ten Poincaré generators. Indeed, the maximum number of kinematic generators allowed in any form of relativistic dynamics is seven and the LFD is the only one that possesses this maximum number of kinematic generators. Effectively, the LFD maximizes the capacity to describe hadrons by saving a lot of dynamical efforts in obtaining the QCD solutions that reflect the full Poincaré symmetries.

Among these three forms of dynamics proposed by Dirac, the two forms of dynamics, IFD and LFD, can be linked to each other [6]. We have discussed the correspondence between the LFD and the IFD, which has been the traditional approach, using an interpolation angle parameter spanning between the IFD and LFD. We may summarize the interpolation between IFD and LFD as well as its applications in the last few decades as illustrated in Fig. 1. There have been earlier works closely related to this subject, using a tilted coordinate near the light-front time axis to quantize the fields slightly away from the light-front [7–9]. In particular, the work of Ref. [9] was concerning the role of light-front zero-modes in QED and QCD with respect to the confinement and chiral symmetry of QCD in contrast to QED.

In our interpolation between the IFD and LFD [6], we maintain the orthogonality of the coordinate system in the process of interpolation to correspond the quantum field theories between the IFD and the LFD as depicted

[a] e-mail: crji@ncsu.edu (corresponding author)

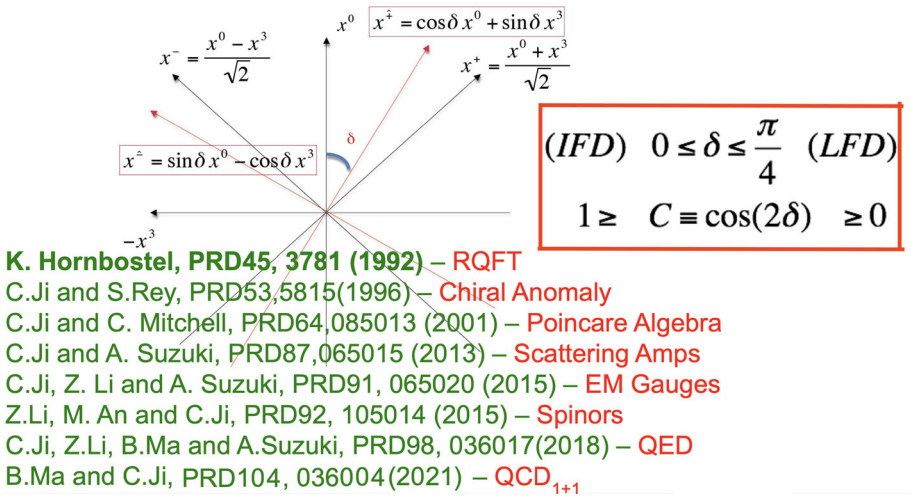

Fig. 1 Interpolation between IFD and LFD and references with topics of applications

in Fig. 1. Although we want ultimately to obtain a general formulation for the QCD, we started from a simpler theory to discuss first the bare-bone structure that will persist even in the more complicated theories. Starting from the scalar field theory [10] to discuss the interpolating scattering amplitude with only momentum degree of freedom, we have extended the discussion to the electromagnetic gauge degree of freedom [11] and the on-mass-shell fermion [12]. In particular, we discussed the link between the Coulomb gauge in IFD and the light-front gauge in LFD [11] and the chiral representation of the helicity spinors interpolating between the IFD and the LFD [12]. We have also entwined the fermion propagator interpolation with our previous works on the electromagnetic gauge field [11] and the helicity spinors [12] and fasten the bolts and nuts necessary to launch the interpolating QED [13]. While we have discussed the prototype of QED scattering processes "$e\mu \to e\mu$" and "$e^+e^- \to \mu^+\mu^-$" involving a photon propagator in our previous work [12], we presented the two-photon production amplitude in the pair annihilation of fermion and anti-fermion process "$e^+e^- \to \gamma\gamma$" as well as the Compton scattering amplitude "$e\gamma \to e\gamma$" involving a fermion propagator in our landmark paper on interpolating QED [13]. We have discussed the intermediate fermion propagator in Ref. [13] as a further development from the study of external fermions and bosons which have already been discussed in Ref. [11, 12]. Subsequently, we have interpolated the 'tHooft model between IFD and LFD [14]. In this review, we illustrate the interpolation between IFD and LFD and demonstrate explicit examples of its utility in QED and QCD.

2 Interpolation between IFD and LFD

To trace the forms of relativistic quantum field theory between IFD and LFD, we take the following convention of the space-time coordinates to define the interpolation angle [10–12, 15, 16]:

$$\begin{bmatrix} x^{\hat{+}} \\ x^{\hat{-}} \end{bmatrix} = \begin{bmatrix} \cos\delta & \sin\delta \\ \sin\delta & -\cos\delta \end{bmatrix} \begin{bmatrix} x^0 \\ x^3 \end{bmatrix}, \tag{1}$$

in which the interpolation angle is allowed to run from 0 through 45°, $0 \le \delta \le \frac{\pi}{4}$. The lower index variables $x_{\hat{+}}$ and $x_{\hat{-}}$ are related to the upper index variables as $x_{\hat{+}} = g_{\hat{+}\hat{\mu}}x^{\hat{\mu}} = \mathbb{C}x^{\hat{+}} + \mathbb{S}x^{\hat{-}}$ and $x_{\hat{-}} = g_{\hat{-}\hat{\mu}}x^{\hat{\mu}} = -\mathbb{C}x^{\hat{-}} + \mathbb{S}x^{\hat{+}}$, denoting $\mathbb{C} = \cos2\delta$ and $\mathbb{S} = \sin2\delta$ and realizing $g_{\hat{+}\hat{+}} = -g_{\hat{-}\hat{-}} = \cos2\delta = \mathbb{C}$ and $g_{\hat{+}\hat{-}} = g_{\hat{-}\hat{+}} = \sin2\delta = \mathbb{S}$. All the indices with the wide-hat notation signify the variables with the interpolation angle δ. For the limit $\delta \to 0$ we have $x^{\hat{+}} = x^0$ and $x^{\hat{-}} = -x^3$ so that we recover usual space-time coordinates although the z-axis is inverted while for the other extreme limit, $\delta \to \frac{\pi}{4}$, we have $x^{\hat{\pm}} = (x^0 \pm x^3)/\sqrt{2} \equiv x^{\pm}$ which leads to the standard light-front coordinates. Since the perpendicular components remain the same ($x^{\hat{j}} = x^j$, $x_{\hat{j}} = x_j$, $j = 1, 2$), we will omit the "$\hat{}$" notation unless necessary from now on for the perpendicular indices $j = 1, 2$ in a four-vector. Of course, the same interpolation applies to the four-momentum variables too as it applies to all four-vectors. The details of the relationship between the interpolating variables and the usual space-time variables can be seen in our previous works Refs. [10–12].

2.1 Interpolating scattering amplitudes

As a simple illustration of our interpolation between IFD and LFD, we discussed [10] the scattering amplitude of two spin-less particles, e.g. an analogue of the well-known QED annihilation/production process $e^+e^- \to \mu^+\mu^-$ in a toy ϕ^3 model theory, as depicted in Fig.2. In Ref. [10], we do not involve spins and any other degrees of freedom except the fundamental degrees of freedom, i.e. particle momenta, for the simplest possible illustration.

Although we discussed there [10] just this simple scattering amplitude, the bare-bone structure that we demonstrate in this analysis will be commonly applicable to any further complicated amplitudes including other degrees of freedom. In particular, the main points that we discuss from the energy denominator structure in this simple amplitude will prevail in other complicated amplitudes since not only the basic structure of the amplitudes, but also the fundamental degrees of freedom to describe the scattering process are applicable to any quantum field theories. Further complications from other degrees of freedom beyond the particle momenta would appear separately without modifying the energy denominator structure that we discuss in this subsection. For example, the terms associated with the spin degrees of freedom in QED would appear as the matrix elements in the numerator but not in the denominator of the amplitude. The extension of the present work to the gauge field theories involving other degrees of freedom, such as QED and QCD has been illustrated in Refs. [13, 14], respectively. In this subsection, we will focus on the basic structure of the scattering amplitudes, i.e. the energy denominators, considering only the fundamental degrees of freedom, i.e. particle momenta.

Modulo inessential factors including the square of the coupling constant, the lowest order tree-level Feynman diagram shown in Fig. 2 is proportional to the propagator of the intermediate particle, that is,

$$\Sigma = \frac{1}{s - m^2}, \tag{2}$$

where $s = (p_1 + p_2)^2$ is the Mandelstam variable which is invariant under any Poincaré transformations and m is the mass of the intermediate boson. Of course, the physical process can take place only above the threshold $s > 4M^2$, where M is the mass of the final particle and anti-particle that are produced, e.g. like the muon mass in the $e^+e^- \to \mu^+\mu^-$ scatterring process. In the instant form dynamics (IFD), where the initial conditions are set on the hyperplane $t = 0$ and the system evolves with the ordinary time $t > 0$, this manifestly covariant Feynman amplitude is decomposed into the corresponding two time-ordered amplitudes, graphically represented in Fig. 3a, b.

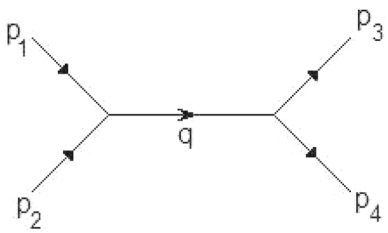

Fig. 2 Scattering amplitude of spinless particles analogous to $e^+e^- \to \mu^+\mu^-$

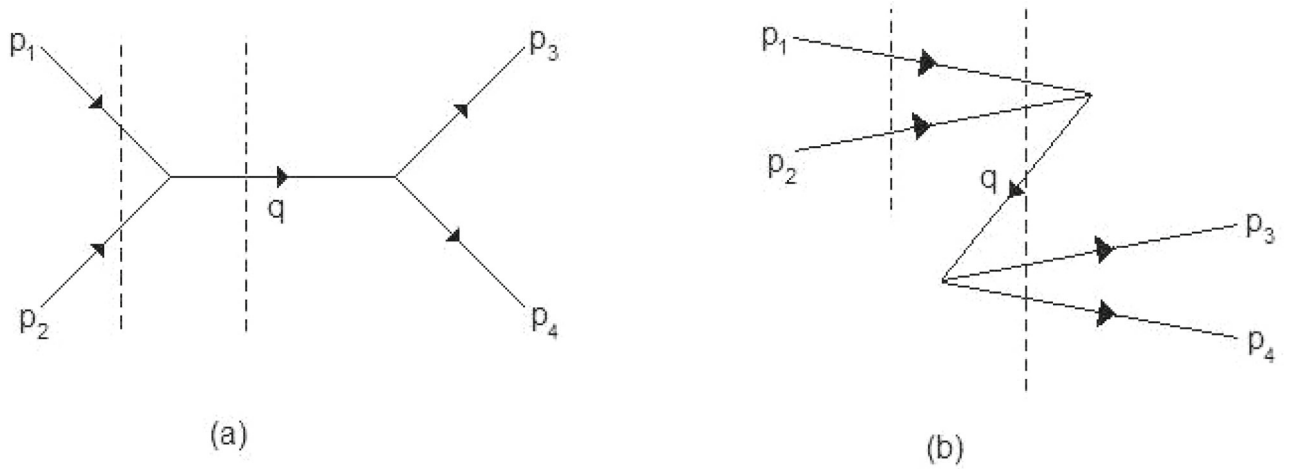

Fig. 3 Time-ordered amplitudes in IFD for the Feynman amplitude depicted in Fig. 2

These two time-ordered amplitudes correspond, respectively, to the following analytic expressions:

$$\Sigma^a_{\rm IFD} = \frac{1}{2q^0}\left(\frac{1}{p_1^0+p_2^0-q^0}\right), \tag{3}$$

and

$$\Sigma^b_{\rm IFD} = -\frac{1}{2q^0}\left(\frac{1}{p_1^0+p_2^0+q^0}\right). \tag{4}$$

It is not difficulty to show that the sum of the time-ordered amplitudes is identical to the manifestly covariant Feynman amplitude:

$$\begin{aligned}\Sigma_{\rm IFD} =&\Sigma^{\rm IFD}_a + \Sigma^{\rm IFD}_b \\ =&\frac{1}{2q^0}\left(\frac{1}{p_1^0+p_2^0-q^0} - \frac{1}{p_1^0+p_2^0+q^0}\right) \\ =&\frac{1}{s-m^2},\end{aligned} \tag{5}$$

where the conservation of the three momentum $\vec{p}_1+\vec{p}_2=\vec{q}$ as well as the energy-momentum dispersion relation $q^0=\sqrt{\vec{q}^2+m^2}$ in IFD is used to get the covariant denominator $s-m^2$ in the last step.

To obtain the corresponding time-ordered amplitudes in an arbitrary interpolating angle δ, we just need to change the superscript 0 of the IFD energy variables in the energy denominators to the superscript $\hat{+}$ and multiply an overall factor $\mathbb{C}$ to the amplitudes: i.e.

$$\Sigma^a_\delta = \frac{1}{2q^{\widehat{+}}}\left(\frac{\mathbb{C}}{p_1^{\widehat{+}}+p_2^{\widehat{+}}-q^{\widehat{+}}}\right), \tag{6}$$

and

$$\Sigma^b_\delta = -\frac{1}{2q^{\widehat{+}}}\left(\frac{\mathbb{C}}{p_1^{\widehat{+}}+p_2^{\widehat{+}}+q^{\widehat{+}}}\right). \tag{7}$$

The overall factor $\mathbb{C}$ is necessary because the physical energy of the particle with the four-momentum $p^{\widehat{\mu}}$ in an arbitrary interpolation angle is given by $p_{\widehat{+}}$ and as one can see $p^{\widehat{+}}=\mathbb{C}p_{\widehat{+}}+\mathbb{S}p_{\widehat{-}}$ should be used to evaluate the interpolating amplitudes. Note here that the factor $\mathbb{S}$ in front of the longitudinal momentum $p_{\widehat{-}}$ is irrelevant because the longitudinal momenta of the initial particles must be cancelled by the longitudinal momentum of the intermediate particle due to the conservation of longitudinal momentum. Again, it is not so difficulty to show that the sum of the time-ordered amplitudes for any angle δ is identical to the manifestly covariant Feynman amplitude:

$$\begin{aligned}\Sigma_\delta =&\Sigma^a_\delta + \Sigma^b_\delta \\ =&\frac{1}{2q^{\widehat{+}}}\left(\frac{\mathbb{C}}{p_1^{\widehat{+}}+p_2^{\widehat{+}}-q^{\widehat{+}}} - \frac{\mathbb{C}}{p_1^{\widehat{+}}+p_2^{\widehat{+}}+q^{\widehat{+}}}\right) \\ =&\frac{1}{s-m^2},\end{aligned} \tag{8}$$

where we used the relation between the covariant and contravariant indices such as $q^{\widehat{+}}=\mathbb{C}q_{\widehat{+}}+\mathbb{S}q_{\widehat{-}}$ and the conservation of momenta $p_{1\widehat{-}}+p_{2\widehat{-}}=q_{\widehat{-}}$ and $\vec{\mathbf{p}}_{1\widehat{\perp}}+\vec{\mathbf{p}}_{2\widehat{\perp}}=\vec{\mathbf{q}}_{\widehat{\perp}}$ as well as the four-momentum scalar product relation to get the covariant denominator $s-m^2$ in the last step. It is also rather easy to see that Eq. (8) becomes Eq. (5) as $\mathbb{C}$ goes to the unity. In LFD however, i.e. as $\mathbb{C}$ goes to zero, the denominator in the first amplitude $\Sigma^a_{\delta=\pi/4}$, i.e. $1/(p_1^{\widehat{+}}+p_2^{\widehat{+}}-q^{\widehat{+}})=1/(p_1^+ + p_2^+ - q^+)$ goes to infinity due to the conservation $p_1^+ + p_2^+ = q^+$ but the multiplication of $\mathbb{C}=0$ with this infinity makes the finite result $1/(s-m^2)$, while the second amplitude $\Sigma^b_{\delta=\pi/4}$ is wiped out due to $\mathbb{C}=0$. This result is akin to the very well-known result from the work "Dynamics at Infinite Momentum" [17]. However, we would like to make it clear that the disappearance of the second amplitude $\Sigma^b_{\delta=\pi/4}$

in LFD is different from what has been known from IMF, i.e. when $P_z \to \pm\infty$ with $P \equiv p_1 + p_2$ for a shorthand notation (e.g. $P^2 = s$). As far as any correlation between the interpolation angle δ and the total longitudinal momentum P_z is avoided, our derivation is completely independent of the frame and the only relevant parameter to show this disappearance is the interpolation angle δ, which has nothing to do with the choice of reference frame. As discussed in Ref. we paid attention to the special case with a particular correlation between δ and P_z and the associated treacherous point similar to the zero-mode issue in LFD.

We may elaborate on more details of our derivations discussed above as follows. The dispersion relation $q^2 = m^2$ in terms of interpolating angle variables results in a quadratic equation in $q_{\widehat{+}}$ and $q_{\widehat{-}}$ that can be solved for the energy variable $q_{\widehat{+}}$ in terms of momentum components $q_{\widehat{-}}$ and $\vec{\mathbf{q}}_{\widehat{\perp}}$ as well as mass m:

$$q_{\widehat{+}} = \frac{-\mathbb{S}q_{\widehat{-}} \pm \omega_q}{\mathbb{C}}, \tag{9}$$

in which we introduced the notation

$$\omega_q = \sqrt{q_{\widehat{-}}^2 + \mathbb{C}\left(\vec{\mathbf{q}}_{\widehat{\perp}}^2 + m^2\right)}. \tag{10}$$

For the physical solution with positive energy in Eq. (9), we must take

$$q_{\widehat{+}} = \frac{-\mathbb{S}q_{\widehat{-}} + \omega_q}{\mathbb{C}}, \tag{11}$$

which identifies ω_q as

$$\omega_q = \mathbb{C}q_{\widehat{+}} + \mathbb{S}q_{\widehat{-}} = q^{\widehat{+}}\,. \tag{12}$$

For $\delta = 0$ and $\delta = \frac{\pi}{4}$, ω_q becomes $q^0 = \sqrt{\vec{\mathbf{q}}^2 + m^2}$ and $q^+ = q^0 + q^3$, respectively. Using this variable ω_q, we may rewrite Eqs. (6) and (7) as follows:

$$\begin{aligned} \Sigma_\delta^a =& \frac{1}{2\omega_q D_+} \\ \Sigma_\delta^b =& \frac{1}{2\omega_q D_-}, \end{aligned} \tag{13}$$

where

$$\begin{aligned} D_+ =& P_{\widehat{+}} + \frac{\mathbb{S}q_{\widehat{-}} - \omega_q}{\mathbb{C}} \\ D_- =& P_{\widehat{+}} + \frac{\mathbb{S}q_{\widehat{-}} + \omega_q}{\mathbb{C}}\,, \end{aligned} \tag{14}$$

in which we used the momentum conservation $P_{\widehat{-}} = (p_1)_{\widehat{-}} + (p_2)_{\widehat{-}} = q_{\widehat{-}}$. The sum of both contributions given by Eq. (8) can then be expressed as

$$\begin{aligned} \Sigma_\delta =& \Sigma_\delta^a + \Sigma_\delta^b \\ =& \frac{1}{2\omega_q}\left(\frac{1}{P_{\widehat{+}} + \frac{\mathbb{S}q_{\widehat{-}} - \omega_q}{\mathbb{C}}} - \frac{1}{P_{\widehat{+}} + \frac{\mathbb{S}q_{\widehat{-}} + \omega_q}{\mathbb{C}}}\right), \end{aligned} \tag{15}$$

which is identical to the second line of Eq. (8). In Eq. (15), we can confirm $\Sigma_\delta = 1/(s - m^2)$:

$$\begin{aligned} \Sigma_\delta =& \frac{\frac{1}{\mathbb{C}}}{\left(P_{\widehat{+}} + \frac{\mathbb{S}q_{\widehat{-}}}{\mathbb{C}}\right)^2 - \left(\frac{\omega_q}{\mathbb{C}}\right)^2} \\ =& \frac{1}{\mathbb{C}P_{\widehat{+}}^2 + 2\mathbb{S}P_{\widehat{+}}q_{\widehat{-}} + \frac{\mathbb{S}^2 q_{\widehat{-}}^2}{\mathbb{C}} - \frac{\omega_q^2}{\mathbb{C}}} \end{aligned}$$

$$
\begin{aligned}
&= \frac{1}{\mathbb{C}P_{\widehat{+}}^2 + 2\mathbb{S}P_{\widehat{+}}P_{\widehat{-}} - \mathbb{C}P_{\widehat{-}}^2 - \vec{\mathbf{P}}_{\widehat{\perp}}^2 - m^2} \\
&= \frac{1}{s - m^2}\,,
\end{aligned} \tag{16}
$$

where we used $\omega_q^2 = q_{\widehat{-}}^2 + \mathbb{C}(\vec{\mathbf{q}}_{\widehat{\perp}}^2 + m^2)$, $P_{\widehat{-}} = q_{\widehat{-}}$ and $\vec{\mathbf{P}}_{\widehat{\perp}} = \vec{\mathbf{q}}_{\widehat{\perp}}$. Using Eq. (15), we may now recapture the instant form and light-front limits, as follows.

For the instant form limit (IFD), we have $\delta \to 0$ (i.e. $\mathbb{C} \to 1$ and $\mathbb{S} \to 0$) and $\omega_q \to q_{\widehat{+}}$. In this limit, it is apparent that Eq. (15) becomes

$$
\Sigma_{\delta\to 0} \equiv \Sigma_{IFD} = \frac{1}{2q_{\widehat{+}}}\left(\frac{1}{P_{\widehat{+}} - q_{\widehat{+}}} - \frac{1}{P_{\widehat{+}} + q_{\widehat{+}}}\right) = \frac{1}{2q_0}\left(\frac{1}{P_0 - q_0} - \frac{1}{P_0 + q_0}\right), \tag{17}
$$

where $\delta = 0$ is taken in the interpolating angle variables as given by Eq. (11).

For the light-front limit (LFD), $\delta \to \frac{\pi}{4}$ (i.e. $\mathbb{C} \to 0$ and $\mathbb{S} \to 1$), we expand ω_q given by Eq. (10) in the orders of $\mathbb{C}$ and get

$$
\omega_q \to q_{\widehat{-}} + \frac{\mathbb{C}\left(\vec{\mathbf{q}}_{\widehat{\perp}}^2 + m^2\right)}{2q_{\widehat{-}}} + \mathcal{O}(\mathbb{C}^2). \tag{18}
$$

Substituting this expansion of ω_q in the denominator of the first term in Eq. (15), we get

$$
\begin{aligned}
\frac{\mathbb{S}q_{\widehat{-}} - \omega_q}{\mathbb{C}} &\to -\frac{\vec{\mathbf{q}}_{\widehat{\perp}}^2 + m^2}{2q_{\widehat{-}}} + \mathcal{O}(\mathbb{C}) \\
&\to -\frac{\vec{\mathbf{q}}_{\widehat{\perp}}^2 + m^2}{2q_{\widehat{-}}} \quad \text{as } \mathbb{C} \to 0.
\end{aligned} \tag{19}
$$

For the second denominator in Eq. (15), however, we get

$$
\begin{aligned}
\frac{\mathbb{S}q_{\widehat{-}} + \omega_q}{\mathbb{C}} &\to \frac{2}{\mathbb{C}} - \frac{\vec{\mathbf{q}}_{\widehat{\perp}}^2 + m^2}{2q_{\widehat{-}}} + \mathcal{O}(\mathbb{C}) \\
&\to \infty \quad \text{as } \mathbb{C} \to 0.
\end{aligned} \tag{20}
$$

Thus, in the light-front limit ($\mathbb{C} \to 0$), the contribution from the second diagram vanishes and

$$
\Sigma_{\delta\to\frac{\pi}{4}} = \frac{1}{2q_{\widehat{-}}}\frac{1}{\left\{P_{\widehat{+}} - \frac{(\vec{\mathbf{q}}_{\widehat{\perp}}^2 + m^2)}{2q_{\widehat{-}}}\right\}} = \frac{1}{P^+}\frac{1}{\left\{P^- - \frac{(\vec{\mathbf{P}}_{\widehat{\perp}}^2 + m^2)}{2P^+}\right\}}\,, \tag{21}
$$

where $q_{\widehat{-}} \to q_- = q^+$ and $\vec{\mathbf{q}}_{\widehat{\perp}} \to \vec{\mathbf{q}}_\perp$ are same with P^+ and $\vec{\mathbf{P}}_\perp$, respectively, due to the momentum conservation in LFD. Again, we would like to make it clear that the disappearance of the second amplitude $\Sigma^b_{\delta=\pi/4}$ in LFD is different from what has been known from the IMF, i.e. when $P_z \to \pm\infty$. The longitudinal boost is kinematic in LFD so that the disappearance of the connected contribution $\Sigma^b_{\delta\to\frac{\pi}{4}}$ to the current arising from the vacuum is independent of P_z or the IMF. This is certainly not the case for any other interpolation case, i.e. $\delta \neq \pi/4$. The longitudinal boost becomes dynamic for $\delta \neq \pi/4$ and the contributions from Σ^a_δ and Σ^b_δ depend on P_z (or the reference frames) and the well-known utility of IMF can be extended to an arbitrary interpolating angle $0 \leq \delta < \frac{\pi}{4}$. The profiles of the landscape of Σ^a_δ and Σ^b_δ in the space of δ and P_z are shown in Fig. 4. More details of the discussion on the interpolating scattering amplitudes can be found in Ref. [10]. In particular, the matrix of the homogeneous part of Poincaré group in the interpolating angle basis may be written as

$$
M_{\widehat{\mu}\widehat{\nu}} = \begin{bmatrix} 0 & K^3 & \mathcal{D}^{\widehat{1}} & \mathcal{D}^{\widehat{2}} \\ -K^3 & 0 & \mathcal{K}^{\widehat{1}} & \mathcal{K}^{\widehat{2}} \\ -\mathcal{D}^{\widehat{1}} & -\mathcal{K}^{\widehat{1}} & 0 & J^3 \\ -\mathcal{D}^{\widehat{2}} & -\mathcal{K}^{\widehat{2}} & -J^3 & 0 \end{bmatrix} \tag{22}
$$

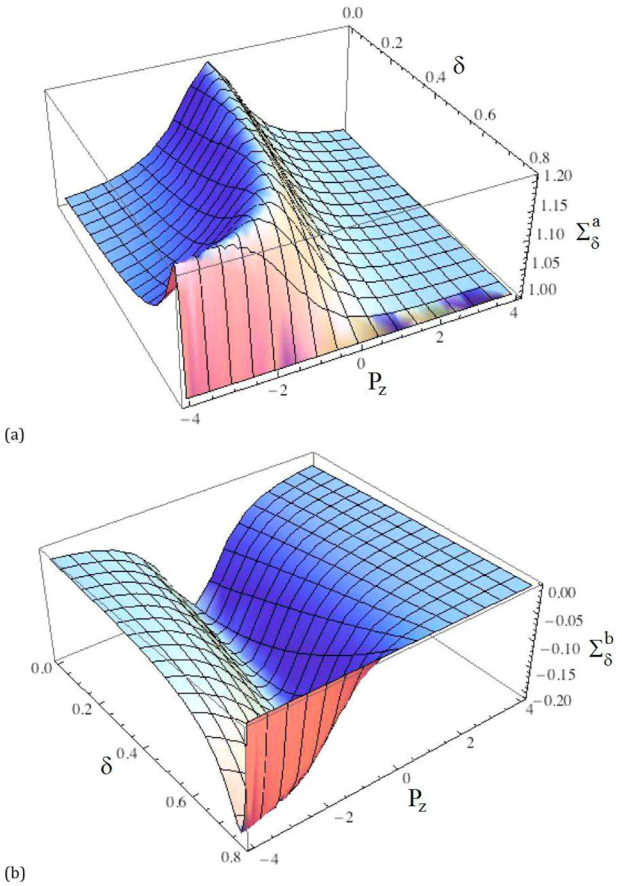

Fig. 4 Landscape of the interpolating amplitudes Σ^a_δ and Σ^b_δ

where

$$\begin{aligned}\mathcal{K}^{\widehat{1}} &= -K^1\sin\delta - J^2\cos\delta; \mathcal{K}^{\widehat{2}} = J^1\cos\delta - K^2\sin\delta\\ \mathcal{D}^{\widehat{1}} &= -K^1\cos\delta + J^2\sin\delta; \mathcal{D}^{\widehat{2}} = -J^1\sin\delta - K^2\cos\delta\,.\end{aligned} \tag{23}$$

The kinematic generators $\mathcal{K}^{\widehat{j}}$ and the dynamic ones $\mathcal{D}^{\widehat{j}}$, $j = (1,\ 2)$, can also be written as the combinations of $E^{\widehat{j}}$ and $F^{\widehat{j}}$:

$$\begin{aligned}\mathcal{K}^{\widehat{1}} &= \mathbb{C}F^{\widehat{1}} - \mathbb{S}E^{\widehat{1}}; \mathcal{K}^{\widehat{2}} = \mathbb{C}F^{\widehat{2}} - \mathbb{S}E^{\widehat{2}}\\ \mathcal{D}^{\widehat{1}} &= -\mathbb{S}F^{\widehat{1}} - \mathbb{C}E^{\widehat{1}}; \mathcal{D}^{\widehat{2}} = -\mathbb{S}F^{\widehat{2}} - \mathbb{C}E^{\widehat{2}}\,,\end{aligned} \tag{24}$$

where

$$\begin{aligned}E^{\widehat{1}} &= J^2\sin\delta + K^1\cos\delta; E^{\widehat{2}} = K^2\cos\delta - J^1\sin\delta\\ F^{\widehat{1}} &= K^1\sin\delta - J^2\cos\delta; F^{\widehat{2}} = J^1\cos\delta + K^2\sin\delta\,.\end{aligned} \tag{25}$$

The interpolating operators $E^{\widehat{j}}$ and $F^{\widehat{j}}$ coincide with the usual E^j and F^j of LFD in the limit $\delta = \pi/4$. The transverse boosts $(K^1,\ K^2)$ are dynamic whereas the transverse rotations $(J^1,\ J^2)$ are kinematic in IFD $(\delta = 0)$, while the LF transverse boosts $(E^1,\ E^2)$ are kinematic whereas the LF transverse rotations $(F^1,\ F^2)$ are dynamic in LFD $(\delta = \frac{\pi}{4})$. One may note the swap of the roles between "boosts" and "rotations" in the two forms of relativistic dynamics, IFD and LFD, and utilize it for some hadron phenomenology [46].

2.2 Interpolation of QED and QCD

The interpolation between IFD and LFD can be applied to the relativistic quantum field theories such as QED and QCD. In Ref. [11], we developed the electromagnetic gauge field propagator interpolated between the IFD and the LFD and found that the light-front gauge $A^+ = 0$ in the LFD is naturally linked to the Coulomb gauge $\boldsymbol{\nabla}\cdot\mathbf{A} = 0$ in IFD. We identified the dynamical degrees of freedom for the electromagnetic gauge fields as the transverse photon fields and clarified the equivalence between the contribution of the instantaneous interaction and the contribution from the longitudinal polarization of the virtual photon. Our results for the gauge propagator and time-ordered diagrams clarified whether one should choose the two-term form [18] or the three-term form [19–21] for the gauge propagator in LFD. There has been a sustained interest and discussion on this issue of the two-term vs. three-term gauge propagator in LFD [22]. Our transverse photon propagator in LFD assumes the three-term form, but the third term cancels the instantaneous interaction contribution. Thus, one can use the two-term form of the gauge propagator for effective calculation of amplitudes if one also omits the instantaneous interaction from the Hamiltonian. But if one wants to show equivalence to the covariant theory, all three terms should be kept because the instantaneous interaction is a natural result of the decomposition of Feynman diagrams, and the third term in the propagator is necessary for the total amplitudes to be covariant. We also see that the photon propagator was derived according to the generalized gauge that links the Coulomb gauge to light-front gauge and thus the three-term form appears appropriate to be consistent with the appropriate gauge.

In Ref. [12], we derived the generalized helicity spinor that links the instant form helicity spinor to the light-front helicity spinor. For a given generalized helicity spinor, the spin direction does not coincide with the momentum direction in general. Thus, we studied how the spin orientation angle θ_s changes in terms of both δ and the angle θ that defines the momentum direction of the particle. In particular, the helicity in IFD depends on the reference frame. If the observer moves faster than the positive helicity spinor, then the direction of the momentum becomes opposite to the spin direction and the helicity of the spinor flips its sign. In contrast, the helicity defined in LFD is independent of the reference frame. We have detailed the increment of the angle difference $\theta - \theta_s$ with the increment of the interpolation angle δ in Ref. [12], which bifurcates at a critical interpolation angle δ_c. We found this critical interpolation angle $\delta_c = \arctan\left(\frac{|\mathbf{P}|}{E}\right)$, where $|\mathbf{P}|$ and E are the magnitude of the three-momentum and the energy of the particle under investigation. The IFD and the LFD belong to separately the two different branches bifurcated and divided out at the critical interpolation angle δ_c. This bifurcation indicates the necessity of the distinction in the spin orientation between the IFD and the LFD and clarifies any conceivable confusion in the prevailing notion of the equivalence between the LFD and the infinite momentum frame (IMF) approach [17] formulated in the IFD.

While the generalized helicity spinors are obtained by applying the transformation given by the transformation matrix $T = e^{i\beta_1 \mathcal{K}^{\hat{1}} + i\beta_2 \mathcal{K}^{\hat{2}}} e^{-i\beta_3 K^3}$, where the values of β_1, β_2, β_3 for an interpolation angle δ are related to the desired final momentum $\vec{P} = (P^1, P^2, P^3)$ of the particle with mass M [12], the Dirac spinors which one may call as rotation-less spinors are obtained by directly boosting the initial state at rest that has a spin projection along the z direction to the state with the desired momentum $\vec{P} = (P^1, P^2, P^3)$. The Dirac spinors in IFD are the familiar spinors that show up in many textbooks. In IFD, however, the spin direction of the Dirac spinor is in general not aligned to the moving direction (i.e. the 3-momentum direction or in short the momentum direction) of the particle represented by the same Dirac spinor, while the spin direction of the helicity spinor is always aligned with the momentum direction of the particle represented by the same helicity spinor. One should note that the boost operation to get the Dirac spinors is entirely dynamical in contrast to the helicity spinors, which would be the case even if the interpolation angle δ is away from the IFD. Although one may still consider such an interpolating Dirac spinor representation for any δ, the operation to get those interpolating Dirac spinors is too dynamical to lend any useful discussion for the general interpolation angle $\delta \neq 0$. Thus, one may prefer relating the light-front spinor to the Jacob-Wick helicity spinor rather than to the rotation-less Dirac spinors although one can still exhibit them for spin $J = \frac{1}{2}$ using the $(0, J) \oplus (J, 0)$ chiral representation [12].

As the spinor was interpolated between IFD and LFD [12], we also showed [13] that the covariant Feynman propagator $\Sigma = \frac{\not{q}+m}{q^2-m^2}$ of the intermediate virtual fermion with the four-momentum q and the mass m can also be decomposed into the two interpolating time-ordered processes, one with the "forward moving" intermediate fermion in the sense that its interpolating longitudinal momentum $q_{\widehat{-}}$ is positive, i.e. $q_{\widehat{-}} > 0$ and the other with the "backward moving" intermediate fermion carrying the opposite sign of $-q_{\widehat{-}}$, i.e. $-q_{\widehat{-}} < 0$. The corresponding "forward" and "backward" amplitudes are given by

$$\Sigma_F = \frac{1}{2Q^{\widehat{+}}} \frac{\not{Q}_F + m}{q_{\widehat{+}} - Q_{F\widehat{+}}}, \Sigma_B = \frac{1}{2Q^{\widehat{+}}} \frac{-\not{Q}_B + m}{-q_{\widehat{+}} - Q_{B\widehat{+}}}, \tag{26}$$

where

$$Q_{F\widehat{+}} = \frac{-\mathbb{S}q_{F\widehat{-}} + Q^{\widehat{+}}}{\mathbb{C}}, \tag{27}$$

$$Q_{B\widehat{+}} = \frac{-\mathbb{S}q_{B\widehat{-}} + Q^{\widehat{+}}}{\mathbb{C}}, \tag{28}$$

and

$$Q^{\widehat{+}} = \sqrt{q_{\widehat{-}}^2 + \mathbb{C}(\mathbf{q}_\perp^2 + m^2)}, \tag{29}$$

with the 4-momenta $q_F = q$ and $q_B = -q$ which are those of the off-shell fermion and anti-fermion, while Q_F and Q_B are the corresponding on-shell 4-momenta. Only the interpolating energies of the "forward" and "backward" moving intermediate fermions, i.e. $Q_{F\widehat{+}}$ and $Q_{B\widehat{+}}$ are different from q_F and q_B, respectively, as given by Eqs. (27) and (28). In the light-front limit $\delta \to \frac{\pi}{4}$, i.e., $\mathbb{C} \to 0$, we get

$$\Sigma_{F,\,\delta\to\frac{\pi}{4}} = \frac{\not{q}_{on} + m}{q^2 - m^2}, \qquad \Sigma_{B,\,\delta\to\frac{\pi}{4}} = \frac{\gamma^+}{2q^+}, \tag{30}$$

where q_{on} is the on-shell momentum 4-vector with its spacial part equal to that of q while it satisfies the Einstein energy-momentum relationship. Here, $\Sigma_{B,\,\delta\to\frac{\pi}{4}}$ turns out to be the instantaneous contribution in the light-front propagator. This proves the usual light-front decomposition of the fermion propagator given by [23]

$$\frac{1}{\not{q} - m} = \frac{\sum_s u(q,\,s)\bar{u}(q,\,s)}{q^2 - m^2} + \frac{\gamma^+}{2q^+}, \tag{31}$$

where the numerator $\not{q}_{on} + m$ of $\Sigma_{F,\,\delta\to\frac{\pi}{4}}$ in Eq. (30) is replaced by the spin sum of the on-shell spinor product $\sum_s u(q,\,s)\bar{u}(q,\,s)$.

Moreover, we presented the formal derivation of the interpolating QED [13]. We outlined two different derivations of the Feynman rules for $x^{\widehat{+}}$-ordered diagrams formulated at any interpolation angle. The first approach directly decomposed the covariant Feynman diagram, and the second one utilized the canonical field theory and the old-fashioned perturbation theory. We noticed in particular the constraint fermion degree of freedom, which appears uniquely in the LFD, resulting in the instantaneous contribution to the fermion propagator. The canonical field theory was studied for the entire range of the interpolation angle $0 \le \delta \le \pi/4$. Equations of motion, free fields, gauge condition, momentum and angular momentum tensor were examined, and the Hamiltonian at constant $x^{\widehat{+}}$ was found. We further studied the $x^{\widehat{+}}$-ordered fermion propagator in more detail. Taking a simple example, the annihilation of fermion and anti-fermion into two scalar particles, we showed the characteristic behavior of the amplitudes as the form interpolates between IFD and LFD, and also examined the angular momentum conservation. When we presented the results for the $e^+e^- \to \gamma\gamma$ process and the Compton Scattering $e\gamma \to e\gamma$, we computed all 16 helicity amplitudes and discussed the frame dependence and/or the scattering angle dependence with respect to the interpolation angle dependence. For the $e^+e^- \to \gamma\gamma$ amplitudes, the symmetry between the forward and

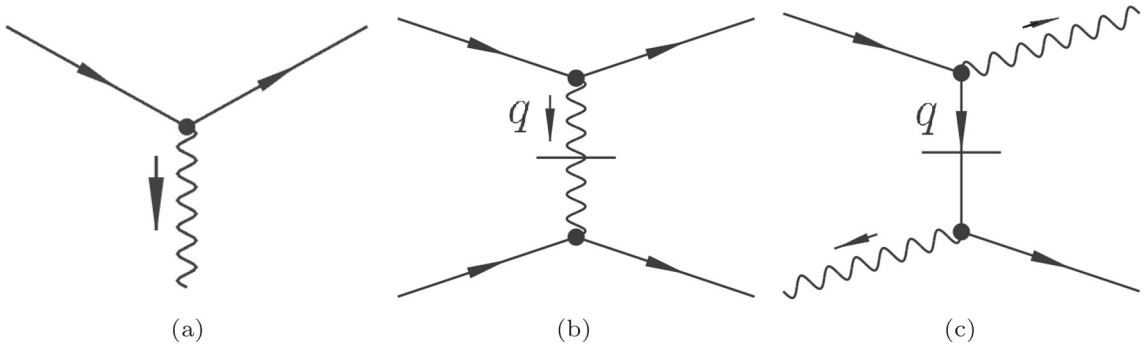

Fig. 5 Vertices that appear in the $x^{\widehat{+}}$-ordered diagrams. When $\mathbb{C} \neq 0$, only two kinds of vertices (a) and (b) exist. When $\mathbb{C} = 0$, all three vertices (a), (b), (c) are present

backward angle dependence was discussed. The limit to the LFD ($\delta = \pi/4$) was analyzed and the comparison with the well-known analytic results from the manifestly covariant calculation was presented. We have also presented the fermion propagator in the position space and derived explicitly the manifestly covariant fermion propagator from the sum of the interpolating time-ordered fermion propagators. A lot more complete discussions of QED can be found in Ref. [13], including the canonical field theory of quantum electrodynamics in any interpolating angle, which reproduced the Feynman rules of QED. We may summarize the rules for $x^{\widehat{+}}$-ordered diagrams of QED as follows:

1. $u(p,\, s)$, $\bar{u}(p,\, s)$, $v(p,\, s)$, $\bar{v}(p,\, s)$, $\epsilon_\mu(p,\, \lambda)$, and $\epsilon^*_\mu(p,\, \lambda)$ for each incoming and outgoing external lines;
2. $(\not{p} + m) = \Sigma_s u(p,\, s)\bar{u}(p,\, s)$ for electron propagators; $(-\not{p} + m) = -\Sigma_s v(p,\, s)\bar{v}(p,\, s)$ for positron propagators; $\mathcal{T}_{\widehat{\mu}\widehat{\nu}} \equiv \sum_{\lambda=\pm} \epsilon^*_{\widehat{\mu}}(\lambda)\epsilon_{\widehat{\nu}}(\lambda)$ for photon propagators;
3. $-ie\gamma^{\widehat{\mu}}\Big(2\pi)^3\delta(P^{\rm in}_{\widehat{-}} - P^{\rm out}_{\widehat{-}}\Big)\delta^2\big(\mathbf{P}^{\rm in}_\perp - \mathbf{P}^{\rm out}_\perp\big)$ for each vertex as shown in Fig. 5a;

$$-e^2\frac{in_{\widehat{\mu}}n_{\widehat{\nu}}}{q^2_{\widehat{-}} + \mathbb{C}\mathbf{q}^2_\perp}(2\pi)^3\delta\Big(P^{\rm in}_{\widehat{-}} - P^{\rm out}_{\widehat{-}}\Big)\delta^2\big(\mathbf{P}^{\rm in}_\perp - \mathbf{P}^{\rm out}_\perp\big)$$
$$\times \cdots\gamma^{\widehat{\mu}}\cdots\gamma^{\widehat{\nu}}\cdots$$

for each vertex as shown in Fig. 5b, where $q_{\widehat{-}}$, $\mathbf{q}_\perp$ are the total momentum transferred;

$$-ie^2\gamma^\mu\gamma^+\gamma^\nu\frac{1}{2q^+}(2\pi)^3\delta\big(P^+_{\rm in} - P^+_{\rm out}\big)\delta^2\big(\mathbf{P}^{\rm in}_\perp - \mathbf{P}^{\rm out}_\perp\big),$$

for each vertex as shown in Fig. 5c appearing only if $\mathbb{C} = 0$, i.e. only in LFD, where $q^+ = k'^+ - p'^+$;

4. $\frac{i}{P_{ini\widehat{+}} - P_{inter\widehat{+}} + \imath\epsilon}$ for each internal line, where $P_{int\widehat{+}}$ and $P_{inter\widehat{+}}$ are the sums of energies for the initial and intermediate particles;
5. an over-all factor of $(2\pi)\delta(P^{in}_{\widehat{+}} - P^{out}_{\widehat{+}})$ for the interpolating energy conservation;
6. an integration

$$\int\frac{\mathrm{d}\mathbf{q}_\perp}{(2\pi)^3}\int_{-\infty}^{\infty}\frac{\mathrm{d}q_{\widehat{-}}}{2Q^{\widehat{+}}}\widehat{\Theta}(q_{\widehat{-}})$$

for every internal propagating line, with m in Eq. (29) being the mass of the exchanged particle.

The gauge corresponding to these $x^{\widehat{+}}$-ordered rules is the generalized transverse gauge $A^{\widehat{+}} = 0$ and $\partial_{\widehat{-}}A_{\widehat{-}} + \boldsymbol{\partial}_\perp \cdot \mathbf{A}_\perp\mathbb{C} = 0$, which links the light-front gauge $A^+ = 0$ in the LFD and the Coulomb gauge $\boldsymbol{\nabla}\cdot\mathbf{A} = 0$ in IFD.

The rules for x^+-ordered diagrams on the light front, first derived by Kogut and Soper [24], are reproduced by taking $\mathbb{C} = 0$ in the above rules. For instance, in rule 6, when $\mathbb{C} = 0$, the integration limits of $q_{\widehat{-}} = q_- = q^+$ change to $(0,\, \infty)$, i.e.

$$\int\frac{\mathrm{d}\mathbf{q}_\perp}{(2\pi)^3}\int_0^{\infty}\frac{\mathrm{d}q^+}{2q^+}$$

for every internal line. The QED rules can be extended to QCD including the color factors. In the next section, we discuss the application of the interpolation to QCD_{1+1} in the large $N_c \to \infty$ limit known as the 't Hooft model. In particular, we discuss the mass gap equation/solution as well as the bound-state equation/solution to lay the ground for the light-front quark model (LFQM) for the phenomenology of hadron physics.

3 Large N_c QCD in 1+1 dimension ('tHooft Model)

With the "hat notation", the theory of QCD_{1+1} in the interpolating quantization is given by the Lagrangian density [1]

$$\mathcal{L} = -\frac{1}{4}F^a_{\hat{\mu}\hat{\nu}}F^{\hat{\mu}\hat{\nu}a} + \bar{\psi}\big(i\gamma^{\hat{\mu}}D_{\hat{\mu}} - m\big)\psi, \tag{32}$$

where

$$D_{\hat{\mu}} = \partial_{\hat{\mu}} - igA^a_{\hat{\mu}}t_a \tag{33}$$

and

$$F^a_{\hat{\mu}\hat{\nu}} = \partial_{\hat{\mu}}A^a_{\hat{\nu}} - \partial_{\hat{\nu}}A^a_{\hat{\mu}} + gf^{abc}A^b_{\hat{\mu}}A^c_{\hat{\nu}}. \tag{34}$$

In 1+1D, the coupling constant g has the mass dimension.

The two-dimensional quantum chromodynamics (QCD_2) with the number of colors $N_c \to \infty$ has served as a theoretical laboratory for the study of strong interactions. In 't Hooft's seminal paper in 1974 [26], the power of $1/N_c$ expansion [27] was demonstrated in solving QCD_2 in the limit of $N_c \to \infty$, which was then widely studied also in relation to the string model and dual theories with the idea of $1/N_c$ expansion as a topological expansion in the motion of physical strings (e.g. by Witten [28]). Under the large N_c approximation, non-planar diagrams are negligible and thus, for example, only the rainbow diagrams need to be summed over for the computation of the quark's self-mass. The two other parameters in QCD_2 besides N_c, are the dimensionful coupling constant g and the quark mass m. Sharing the same mass dimension, g and m play an important role in determining the phase of QCD_2 [29, 30]. Depending on the value of the dimensionless coupling g^2N_c/m^2, it is known that there are at least two phases in QCD_2 [31]. While the regime of the strong coupling phase which doesn't require the finiteness condition on the dimensionless coupling g^2N_c/m^2 [32] can be studied by the bosonization method [33], the regime of the weak coupling phase, which keeps the so-called "'t Hooft coupling" $\lambda \sim g^2N_c$ finite in the limit of not only $N_c \to \infty$ but also $g \to 0$ is investigated typically in QCD_2. Although the strong coupling regime of QCD_2 is interesting and deserves further study, the weak coupling regime of QCD_2 known as the 't Hooft model is highly nontrivial as the theory captures the property of quark confinement and involves the infrared-cutoff procedures discussed in two-dimensional gauge field theories [34, 35].

In Ref. [14], we started from the interpolating Lagrangian density, Eq. (32), derived the corresponding Hamiltonian and solved the mass gap equation, which interpolates between the IFD and the LFD. We then applied the solutions of mass gap equation in the calculations of chiral condensates and the quark-antiquark bound-states to find the meson mass spectra and the corresponding wavefunctions. As expected for any physical observables, the meson mass spectra were found to be independent of the interpolation angle parameter. Since we obtained the meson wavefunctions in terms of the interpolation angle parameter δ, we used these δ-dependent wavefunctions to compute the corresponding parton distribution functions (PDFs), comparing them with the PDFs in the LFD and the so-called quasi-PDFs based on the IMF approach in IFD [36].

In the next subsection, we summarize the fermion mass gap equation in $\mathrm{QCD}_{1+1}(N_c \to \infty)$ in the quantization interpolating between the IFD and the LFD, and the solutions of the mass gap equation numerically spanning the interpolation angle between $\delta = 0$ (IFD) and $\delta = \pi/4$ (LFD). Then, in subsequent subsection, we discuss the quark-antiquark bound-state equations in the interpolating dynamics and present their solutions, including the meson mass spectra, wavefunctions, and (quasi-)PDFs, respectively.

3.1 Mass gap equation and solution

In this section, we summarize the quark self-energy equation in $\mathrm{QCD}_{1+1}(N_c \to \infty)$ in the interpolating dynamics between the IFD and the LFD. While we use two different methods, i.e. the Hamiltonian method and the Feynman-diagram method, we find that both methods provide exactly the same set of equations. When $\delta \to 0$, $\mathbb{C} \to 1$ and

[1] It is worth noting that our definition of g is the same with that of Ref. [25], but differs with that of Ref. [26] by a factor of $\frac{1}{\sqrt{2}}$, i.e., when $\delta \to \frac{\pi}{4}$, (quantities with a superscript "t" denote the notation used in Ref. [26], and the ones without are ours).

$$A^{\mathrm{t}}_\mu = -i\sqrt{2}A^a_\mu t_a, \quad g^{\mathrm{t}} = \frac{1}{\sqrt{2}}g, \quad \text{and} \quad \gamma^{\mathrm{t}}_\mu = -i\gamma^\mu.$$

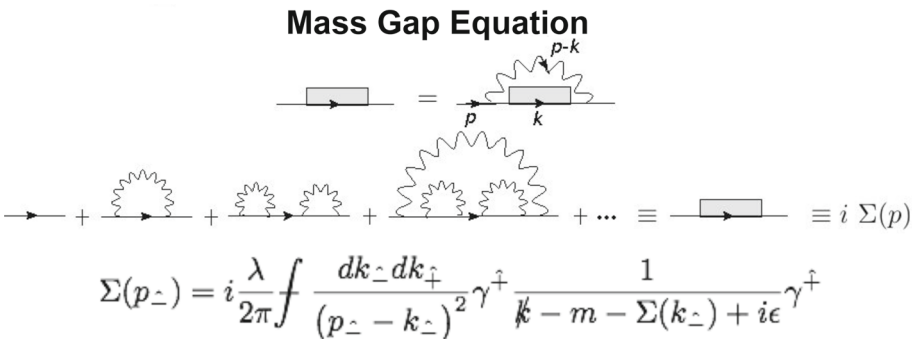

Fig. 6 Fermion self-energy equation in the large N_c limit

$p_\perp \to p^1$, these equations become the IFD mass gap equations presented in Ref. [25]. The agreement to Ref. [26] of the $\delta \to \frac{\pi}{4}$ limit was discussed in Ref. [14].

The self-energy equation in the large N_c approximation is drawn pictorially in Fig. 6. Following the Feynman rules for the gluon propagator, the free quark propagator and the vertex as $\frac{1}{k_\perp^2}$, $\frac{1}{\not{k}-m+i\epsilon}$ and $g\gamma^\hat{+}t^a$, respectively, with the momentum assignment shown in Fig. 6, we have

$$\Sigma(p_\perp) = i\frac{\lambda}{2\pi}\int \frac{\mathrm{d}k_\perp \mathrm{d}k_\hat{+}}{(p_\perp - k_\perp)^2}\gamma^\hat{+}\frac{1}{\not{k} - m - \Sigma(k_\perp) + i\epsilon}\gamma^\hat{+}. \tag{35}$$

Writing the self-energy as

$$\begin{aligned}\Sigma(p_\perp) =& \sqrt{\mathbb{C}}A(p_\perp) + \gamma_\perp B(p_\perp)\\ =& \sqrt{\mathbb{C}}A(p_\perp) + \left(\mathbb{S}\gamma^\hat{+} - \mathbb{C}\gamma^\hat{-}\right)B(p_\perp),\end{aligned} \tag{36}$$

we express the dressed quark propagator as

$$\begin{aligned}S(k) =& \left[\not{k} - m - \Sigma(k_\perp) + i\epsilon\right]^{-1}\\ =& \left[\gamma^\hat{+}\left(k_\hat{+} - \mathbb{S}B(k_\perp)\right) + \gamma^\hat{-}\left(k_\perp + \mathbb{C}B(k_\perp)\right) - \left(m + \sqrt{\mathbb{C}}A(k_\perp)\right) + i\epsilon\right]^{-1}.\end{aligned} \tag{37}$$

This dressed quark propagator can be obtained from the bare quark propagator with the replacement given by

$$\begin{cases} k_\hat{+} \to k_\hat{+} - \mathbb{S}B(k_\perp)\\ k_\perp \to k_\perp + \mathbb{C}B(k_\perp)\\ m \to m + \sqrt{\mathbb{C}}A(k_\perp)\end{cases}. \tag{38}$$

After doing the $k_\hat{+}$ pole integration using Cauchy's theorem, we get

$$\begin{aligned}\Sigma(p_\perp) =& \frac{\lambda}{2}\int \frac{\mathrm{d}k_\perp}{(p_\perp - k_\perp)^2}\frac{\sqrt{\mathbb{C}}\left(\sqrt{\mathbb{C}}m + \mathbb{C}A(k_\perp)\right) + \gamma_\perp\left(k_\perp + \mathbb{C}B(k_\perp)\right)}{\sqrt{\left(k_\perp + \mathbb{C}B(k_\perp)\right)^2 + \left(\sqrt{\mathbb{C}}m + \mathbb{C}A(k_\perp)\right)^2}}\\ =& \frac{\lambda}{2}\int \frac{\mathrm{d}k_\perp}{(p_\perp - k_\perp)^2}\left(\sqrt{\mathbb{C}}\cos\theta(k_\perp) + \gamma_\perp \sin\theta(k_\perp)\right),\end{aligned} \tag{39}$$

where $\theta(k_\perp)$ is defined by

$$\theta(k_\perp) = \tan^{-1}\left[\frac{k_\perp + \mathbb{C}B(k_\perp)}{\sqrt{\mathbb{C}}m + \mathbb{C}A(k_\perp)}\right]. \tag{40}$$

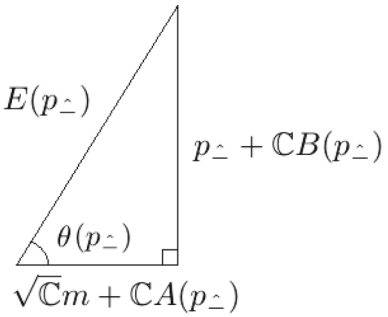

Fig. 7 Geometrical representation of mass gap equations given by Eqs. (43)–(45)

By comparing Eq. (39) with Eq. (36), we can identify

$$A(p_\hat{-}) = \frac{\lambda}{2}\int \frac{\mathrm{d}k_\hat{-}}{\left(p_\hat{-} - k_\hat{-}\right)^2}\cos\theta(k_\hat{-}) \tag{41}$$

and

$$B(p_\hat{-}) = \frac{\lambda}{2}\int \frac{\mathrm{d}k_\hat{-}}{\left(p_\hat{-} - k_\hat{-}\right)^2}\sin\theta(k_\hat{-}). \tag{42}$$

From Eq. (40), we may geometrically represent the effective mass and longitudinal momentum of the particle moving in non-trivial vacuum by drawing the triangle picture shown in Fig. 7.

From Fig. 7, we identify the energy $E(p_\hat{-})$ as

$$E(p_\hat{-})^2 = \left(p_\hat{-} + \mathbb{C}B(p_\hat{-})\right)^2 + \left(\sqrt{\mathbb{C}}m + \mathbb{C}A(p_\hat{-})\right)^2, \tag{43}$$

and find the mass gap equations

$$E(p_\hat{-})\cos\theta(p_\hat{-}) = \sqrt{\mathbb{C}}m + \mathbb{C}\cdot\frac{\lambda}{2}\int \frac{\mathrm{d}k_\hat{-}}{\left(p_\hat{-} - k_\hat{-}\right)^2}\cos\theta(k_\hat{-}), \tag{44}$$

$$E(p_\hat{-})\sin\theta(p_\hat{-}) = p_\hat{-} + \mathbb{C}\cdot\frac{\lambda}{2}\int \frac{\mathrm{d}k_\hat{-}}{\left(p_\hat{-} - k_\hat{-}\right)^2}\sin\theta(k_\hat{-}), \tag{45}$$

where we used Eqs. (41) and (42) for $A(p_\hat{-})$ and $B(p_\hat{-})$.

To discuss the dressed fermion propagator in more physical terms [37], one can express the dressed quark propagator given by Eq. (37) in terms of the mass function $M(p_\hat{-})$ and the wave function renormalization factor $F(p_\hat{-})$, i.e.

$$S(p) = \frac{F(p_\hat{-})}{\not{p} - M(p_\hat{-})}, \tag{46}$$

and identify $M(p_\hat{-})$ and $F(p_\hat{-})$ respectively as

$$M(p_\hat{-}) = p_\hat{-}\frac{m + \sqrt{\mathbb{C}}A(p_\hat{-})}{p_\hat{-} + \mathbb{C}B(p_\hat{-})} = \frac{p_\hat{-}}{\sqrt{\mathbb{C}}}\cot\theta(p_\hat{-}) \tag{47}$$

and

$$F(p_\hat{-}) = \left(1 + \frac{\mathbb{C}B(p_\hat{-})}{p_\hat{-}}\right)^{-1} = \frac{p_\hat{-}}{E(p_\hat{-})\sin\theta(p_\hat{-})}. \tag{48}$$

We then numerically compute $M(p_\hat{-})$ and $F(p_\hat{-})$ using the mass gap solutions $\theta(p_\hat{-})$ and $E(p_\hat{-})$ as shown in Ref. [14].

To comprehend the sign correlation between $F(p_\hat{-})$ and $E(p_\hat{-})$, we write $\cos\theta(p_\hat{-})$ and $\sin\theta(p_\hat{-})$ in terms of $M(p_\hat{-})$ and $F(p_\hat{-})$ from Eqs. (47) and (48), as

$$\cos\theta(p_\hat{-}) = \frac{\sqrt{\mathbb{C}}M(p_\hat{-})}{F(p_\hat{-})E(p_\hat{-})}, \tag{49}$$

and

$$\sin\theta(p_\hat{-}) = \frac{p_\hat{-}}{F(p_\hat{-})E(p_\hat{-})}, \tag{50}$$

so that we may rewrite Eq. (43) associated with the triangle diagram shown in Fig. 7 as

$$F(p_\hat{-})E(p_\hat{-}) = \sqrt{\mathbb{C}M(p_\hat{-})^2 + p_\hat{-}^2}, \tag{51}$$

or

$$E(p_\hat{-}) = \frac{\sqrt{\mathbb{C}M(p_\hat{-})^2 + p_\hat{-}^2}}{F(p_\hat{-})}. \tag{52}$$

In contrast to Eq. (43), we can now express $E(p_\hat{-})$ itself without squaring it as $E(p_\hat{-})^2$ with the support from the wavefunction renormalization factor $F(p_\hat{-})$ as well as the mass function $M(p_\hat{-})$. This is rather remarkable because the issue of $E(p_\hat{-})$ not being always positive for $m \leq 1/\sqrt{\pi} \approx 0.56$ is resolved by expressing the dressed quark propagator $S(p)$ in terms of $F(p_\hat{-})$ and $M(p_\hat{-})$ as given by Eq. (46). While $E(p_\hat{-})$ can be negative, $F(p_\hat{-})E(p_\hat{-})$ is always positive due to the sign correlation between $E(p_\hat{-})$ and $F(p_\hat{-})$ as one can see from Eq. (48) or equivalently from Eq. (50) due to the sign correlation between $\theta(p_\hat{-})$ and $p_\hat{-}$. This allows us to be more physically transparent interpretation of the energy-momentum dispersion relation for the interpolating dressed quark with its self-energy. Moreover, using the rescaled variable $p'_\hat{-} = p_\hat{-}/\sqrt{\mathbb{C}}$, we can assert the interpolation angle independence of the rescaled energy-momentum dispersion given by

$$\frac{F(p'_\hat{-})E(p'_\hat{-})}{\sqrt{\mathbb{C}}} = \sqrt{M(p'_\hat{-})^2 + {p'_\hat{-}}^2} \equiv \tilde{E}(p'_\hat{-}), \tag{53}$$

where we define the interpolation angle independent energy function $\tilde{E}(p'_\hat{-})$ which extends the interpolating energy-momentum dispersion relation of the on-mass-shell particle to the case of the dressed quark with the rescaled variable, i.e.

$$\tilde{E}(p'_\hat{-})^2 = {p'_\hat{-}}^2 + M(p'_\hat{-})^2. \tag{54}$$

As the solution of $\tilde{E}(p_\hat{-})$ is always positive in contrast to $E(p_\hat{-})$, we can now promote the mere pictorial device of geometric interpretation depicted in Fig. 7 to the more physically meaningful geometric interpretation with $\tilde{E}(p'_\hat{-})$, $M(p'_\hat{-})$ and $p'_\hat{-}$ as shown in Fig. 8 with all the positive lengths of the triangle sides. We note the correspondence

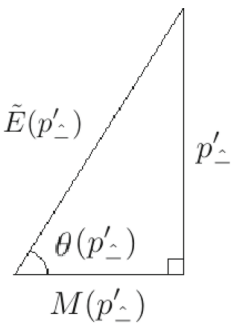

Fig. 8 Geometrical representation of mass gap equations with the interpolation angle independent energy function $\tilde{E}(p'_\hat{-})$ given by Eq. (53)

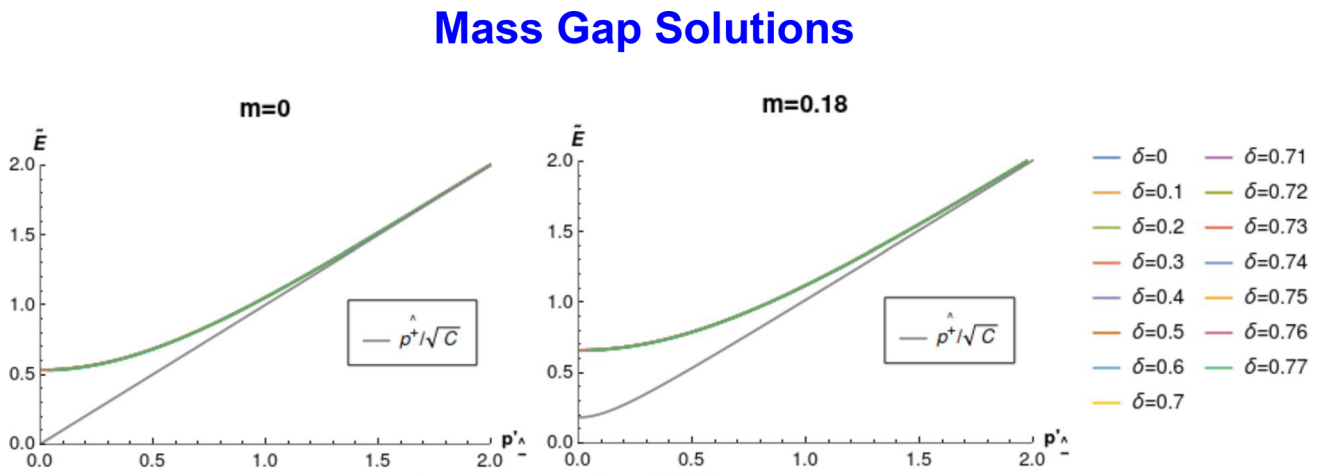

Fig. 9 Interpolation angle independence of mass gap solutions. The curves with different interpolation angles are on top of each other as the interpolating energy-momentum dispersion relation of the on-mass-shell particle given by Eq. (55) is independent of the interpolation angle due to the relativistic form invariance of $\tilde{E}(p'_{\hat{-}})$ and $M(p'_{\hat{-}})$

Table 1 The numerical values of $M(0)$ and $F(0)$ for several different quark mass values

m	0	0.045	0.18	0.749	1.00	2.11	4.23
$M(0)$	0.532778	0.563644	0.659112	1.10105	1.31167	2.30969	4.34358
$F(0)$	−0.495173	−0.584175	−0.987673	4.11079	2.17976	1.22134	1.05526

All quantities are in proper units of $\sqrt{2\lambda}$

$m \leftrightarrow M(p'_{\hat{-}})$ and $p^{\hat{+}}/\sqrt{\mathbb{C}} \leftrightarrow \tilde{E}(p'_{\hat{-}})$ between the bare quark and the dressed quark. As an illustration of this correspondence, we plot the profiles of $\tilde{E}$ as a function of $p'_{\hat{-}}$ for the two cases of $m = 0$ and $m = 0.18$ in Fig. 9. It is evident that $\tilde{E}(p'_{\hat{-}}) \to p^{\hat{+}}/\sqrt{\mathbb{C}}$ as $p'_{\hat{-}} \to \infty$, which is consistent with the result that the mass function $M(p_{\hat{-}})$ approaches the bare quark mass value m as $p_{\hat{-}} \to \infty$.

As $p'_{\hat{-}} \to 0$, however, $\tilde{E}(p'_{\hat{-}})$ approaches the characteristic mass value $M(0)$ as shown in Fig. 9. Indeed, we note $\tilde{E}(0) = \frac{F(0)E(0)}{\sqrt{\mathbb{C}}} = M(0)$, confirming the sign correlation between $E(p_{\hat{-}})$ and $F(p_{\hat{-}})$, i.e. the negativity of $E(p_{\hat{-}})$ for the small $p_{\hat{-}}$ region is compensated by the corresponding negativity of $F(p_{\hat{-}})$ to yield the mass function $M(p_{\hat{-}})$ positive always for any kinematic region of $p_{\hat{-}}$. In Table 1, the numerical values of $M(0)$ and $F(0)$ are tabulated for the quark mass values including the ones shown in Fig. 9. As expected, $F(0)$ values are negative for the small bare quark mass values ($m \lesssim 0.56$) to compensate the corresponding negative values of $E(0)$ while $M(0)$ values are all positive.

3.2 Bound-state equation and solution

Having solved the mass gap equation and obtained the dressed quark propagator interpolating between IFD and LFD, we derived the quark-antiquark bound-state equation in the interpolating form [14]. While we consider the quark-antiquark bound-state with the equal bare mass m in this work, one may generalize it rather straightforwardly to the unequal quark and antiquark mass cases. Bound-states for the unequal quark and antiquark mass cases were analyzed in Refs. [26, 38], and the quark-hadron duality, analytical heavy quark expansion and chiral symmetry breaking effects in the heavy-light mesons have been discussed respectively in Refs. [39–41]. Denoting the covariant Bethe–Salpeter amplitude $\Gamma(r, p)$ of the two-body bound-state with the two-momentum $r^{\hat{\mu}}$ of the bound-state and the two-momentum $p^{\hat{\mu}}$ of one of the two constituents depicted in Fig. 10, we first write down the Bethe-Salpeter equation following the Feynman rules of the gluon propagator and the dressed quark propagator in the 't Hooft model

$$\Gamma(r, p) = \frac{i\lambda}{2\pi} \int \frac{\mathrm{d}k_{\hat{-}}\mathrm{d}k_{\hat{+}}}{(p_{\hat{-}} - k_{\hat{-}})^2} S(p)\gamma^{\hat{+}}\Gamma(r, k)\gamma^{\hat{+}}S(p - r). \tag{55}$$

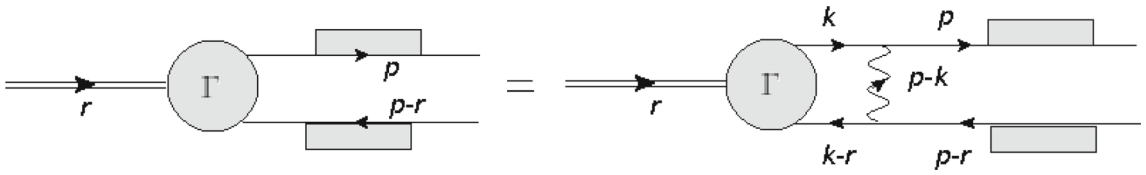

Fig. 10 Diagrammatic representation of the Bethe-Salpeter Equation

To project the covariant Bethe–Salpeter amplitude $\Gamma(r, p)$ into the interpolating equal-time wavefunction, we first integrate out the interpolating energy $p_{\hat{+}}$ and define the wave function $\phi(r_{\hat{-}}, p_{\hat{-}})$ as $\phi(r_{\hat{-}}, p_{\hat{-}}) = \int \mathrm{d}p_{\hat{+}}\Gamma(r, p)$ with the on-mass-shell condition to fix the external interpolating energy $r_{\hat{+}}$. Then, Eq. (55) is converted to the equation for $\phi(r_{\hat{-}}, p_{\hat{-}})$

$$\phi(r_{\hat{-}}, p_{\hat{-}}) = \frac{i\lambda}{2\pi}\int \frac{\mathrm{d}k_{\hat{-}}}{(p_{\hat{-}} - k_{\hat{-}})^2}\int \mathrm{d}p_{\hat{+}} S(p)\gamma^{\hat{+}}\phi(r_{\hat{-}}, k_{\hat{-}})\gamma^{\hat{+}}S(p - r). \tag{56}$$

Now, we also write the fermion propagator $S(p)$ as

$$S(p) = \frac{\tilde{T}(p_{\hat{-}})\Lambda^{+}\tilde{T}^{\dagger}(p_{\hat{-}})\gamma^0}{p_{\hat{+}} - E_u(p_{\hat{-}}) + i\epsilon} + \frac{\tilde{T}(p_{\hat{-}})\Lambda^{-}\tilde{T}^{\dagger}(p_{\hat{-}})\gamma^0}{p_{\hat{+}} - E_v(p_{\hat{-}}) - i\epsilon}, \tag{57}$$

where

$$E_u(p_{\hat{-}}) = -\frac{\mathbb{S}}{\mathbb{C}}p_{\hat{-}} + \frac{E(p_{\hat{-}})}{\mathbb{C}}, \quad E_v(p_{\hat{-}}) = -\frac{\mathbb{S}}{\mathbb{C}}p_{\hat{-}} - \frac{E(p_{\hat{-}})}{\mathbb{C}}, \tag{58}$$

and $u(p_{\hat{-}})\bar{u}(p_{\hat{-}})$ and $v(-p_{\hat{-}})\bar{v}(-p_{\hat{-}})$ are rewritten as

$$u(p_{\hat{-}})\bar{u}(p_{\hat{-}}) = T(p_{\hat{-}})u^{(0)}(0)u^{(0)\dagger}(0)T^{\dagger}(p_{\hat{-}})\gamma^0 = \tilde{T}(p_{\hat{-}})\Lambda^{+}\tilde{T}^{\dagger}(p_{\hat{-}})\gamma^0 \tag{59}$$

and

$$v(-p_{\hat{-}})\bar{v}(-p_{\hat{-}}) = T(p_{\hat{-}})v^{(0)}(p_{\hat{-}}0)v^{(0)\dagger}(p_{\hat{-}}0)T^{\dagger}(p_{\hat{-}})\gamma^0 = \tilde{T}(p_{\hat{-}})\Lambda^{-}\tilde{T}^{\dagger}(p_{\hat{-}})\gamma^0, \tag{60}$$

respectively. Here, we define

$$\Lambda^{+} \equiv \frac{u^{(0)}(0)u^{(0)\dagger}(0)}{2\sqrt{\mathbb{C}}m} = \begin{pmatrix} \frac{1}{2(\cos\delta - \sin\delta)} & \frac{1}{2\sqrt{\mathbb{C}}} \\ \frac{1}{2\sqrt{\mathbb{C}}} & \frac{1}{2(\cos\delta + \sin\delta)} \end{pmatrix} \tag{61}$$

$$\Lambda^{-} \equiv \frac{v^{(0)}(0)v^{(0)\dagger}(0)}{2\sqrt{\mathbb{C}}m} = \begin{pmatrix} \frac{1}{2(\cos\delta - \sin\delta)} & -\frac{1}{2\sqrt{\mathbb{C}}} \\ -\frac{1}{2\sqrt{\mathbb{C}}} & \frac{1}{2(\cos\delta + \sin\delta)} \end{pmatrix} \tag{62}$$

and

$$\tilde{T}(p_{\hat{-}}) = \exp[-\frac{1}{2}\theta(p_{\hat{-}})\frac{\gamma_{\hat{-}}}{\sqrt{\mathbb{C}}}]. \tag{63}$$

Substituting then Eq. (57) to Eq. (56) and performing the $p_{\hat{+}}$ integration, we get

$$\begin{aligned}\phi(r_{\hat{-}}, p_{\hat{-}}) = \lambda\int \frac{\mathrm{d}k_{\hat{-}}}{(p_{\hat{-}} - k_{\hat{-}})^2}\Bigg[&\frac{\tilde{T}(p_{\hat{-}})\Lambda^{+}\tilde{T}^{\dagger}(p_{\hat{-}})\gamma^0\gamma^{\hat{+}}\phi(r_{\hat{-}}, k_{\hat{-}})\gamma^{\hat{+}}\tilde{T}(p_{\hat{-}} - r_{\hat{-}})\Lambda^{-}\tilde{T}^{\dagger}(p_{\hat{-}} - r_{\hat{-}})\gamma^0}{-r_{\hat{+}} + E_u(p_{\hat{-}}) - E_v(p_{\hat{-}} - r_{\hat{-}})} \\ &+ \frac{\tilde{T}(p_{\hat{-}})\Lambda^{-}\tilde{T}^{\dagger}(p_{\hat{-}})\gamma^0\gamma^{\hat{+}}\phi(r_{\hat{-}}, k_{\hat{-}})\gamma^{\hat{+}}\tilde{T}(p_{\hat{-}} - r_{\hat{-}})\Lambda^{+}\tilde{T}^{\dagger}(p_{\hat{-}} - r_{\hat{-}})\gamma^0}{r_{\hat{+}} + E_u(p_{\hat{-}} - r_{\hat{-}}) - E_v(p_{\hat{-}})}\Bigg],\end{aligned} \tag{64}$$

where we note $\tilde{T}(-p_\perp)\tilde{T}(p_\perp) = I$ and further define $\tilde{\phi}(r_\perp, p_\perp) = \tilde{T}(-p_\perp)\phi(r_\perp, p_\perp)\tilde{T}(r_\perp - p_\perp)$, to plug in $\phi(r_\perp, k_\perp) = \tilde{T}(k_\perp)\tilde{\phi}(r_\perp, k_\perp)\tilde{T}(k_\perp - r_\perp)$ and obtain

$$\tilde{\phi}(r_\perp, p_\perp) = \lambda \int \frac{\mathrm{d}k_\perp}{(p_\perp - k_\perp)^2} \left[\frac{\Lambda^+ \tilde{T}^\dagger(p_\perp)\gamma^0\gamma^{\hat{+}}\tilde{T}(k_\perp)\tilde{\phi}(r_\perp, k_\perp)\tilde{T}(k_\perp - r_\perp)\gamma^{\hat{+}}\tilde{T}(p_\perp - r_\perp)\Lambda^-\gamma^0}{-r_{\hat{+}} + E_u(p_\perp) - E_v(p_\perp - r_\perp)} \right.$$
$$\left. + \frac{\Lambda^- \tilde{T}^\dagger(p_\perp)\gamma^0\gamma^{\hat{+}}\tilde{T}(k_\perp)\tilde{\phi}(r_\perp, k_\perp)\tilde{T}(k_\perp - r_\perp)\gamma^{\hat{+}}\tilde{T}(p_\perp - r_\perp)\Lambda^+\gamma^0}{r_{\hat{+}} + E_u(p_\perp - r_\perp) - E_v(p_\perp)} \right]. \tag{65}$$

Examining the general structure of $\tilde{\phi}$ in Eq. (65), we realize that it can be split into the forward moving part $\hat{\phi}_+$ and the backward moving part $\hat{\phi}_-$ with the two 2×2 matrices $\hat{M}^+$ and $\hat{M}^-$, i.e. $\tilde{\phi} = \hat{\phi}_+\hat{M}^+ + \hat{\phi}_-\hat{M}^-$, where

$$\hat{M}^+ = \frac{\gamma^5\sqrt{\mathbb{C}} + \gamma_\perp}{2} = \begin{pmatrix} -\frac{\sqrt{\mathbb{C}}}{2} & \frac{\cos\delta + \sin\delta}{2} \\ -\frac{\cos\delta - \sin\delta}{2} & \frac{\sqrt{\mathbb{C}}}{2} \end{pmatrix}, \tag{66}$$

$$\hat{M}^- = \frac{\gamma^5\sqrt{\mathbb{C}} - \gamma_\perp}{2} = \begin{pmatrix} -\frac{\sqrt{\mathbb{C}}}{2} & -\frac{\cos\delta + \sin\delta}{2} \\ \frac{\cos\delta - \sin\delta}{2} & \frac{\sqrt{\mathbb{C}}}{2} \end{pmatrix}. \tag{67}$$

We note here that $\hat{M}^+$ and $\hat{M}^-$ coincide with the two 2×2 matrices M^+ and M^- in the IFD given by Eq. (4.9) of Ref. [25] as $\delta \to 0$ or $\mathbb{C} \to 1$, i.e. $M^+ = \frac{\gamma^5 + \gamma^1}{2} = \frac{1 + \gamma^0}{2}\gamma^5$, and $M^- = \frac{\gamma^5 - \gamma^1}{2} = \frac{1 - \gamma^0}{2}\gamma^5$, due to $\gamma^0\gamma^5 = \gamma^1$, while $\hat{M}^\pm \to M^\pm_{\mathrm{LF}} = \pm\frac{\gamma^+}{2}$ in the LFD limit $\delta \to \pi/4$ or $\mathbb{C} \to 0$. For the interpolation angle $0 \le \delta \le \pi/4$ in general, from the direct calculation of the matrix multiplications, we find

$$\left[\Lambda^+\tilde{T}^\dagger(p_\perp)\gamma^0\gamma^{\hat{+}}\tilde{T}(k_\perp)\right]\hat{M}^+\left[\tilde{T}(k_\perp - r_\perp)\gamma^{\hat{+}}\tilde{T}(p_\perp - r_\perp)\Lambda^-\gamma^0\right] = C(p_\perp, k_\perp, r_\perp)\hat{M}^+, \tag{68}$$

$$\left[\Lambda^+\tilde{T}^\dagger(p_\perp)\gamma^0\gamma^{\hat{+}}\tilde{T}(k_\perp)\right]\hat{M}^-\left[\tilde{T}(k_\perp - r_\perp)\gamma^{\hat{+}}\tilde{T}(p_\perp - r_\perp)\Lambda^-\gamma^0\right] = -S(p_\perp, k_\perp, r_\perp)\hat{M}^+, \tag{69}$$

$$\left[\Lambda^-\tilde{T}^\dagger(p_\perp)\gamma^0\gamma^{\hat{+}}\tilde{T}(k_\perp)\right]\hat{M}^+\left[\tilde{T}(k_\perp - r_\perp)\gamma^{\hat{+}}\tilde{T}(p_\perp - r_\perp)\Lambda^+\gamma^0\right] = -S(p_\perp, k_\perp, r_\perp)\hat{M}^-, \tag{70}$$

$$\left[\Lambda^-\tilde{T}^\dagger(p_\perp)\gamma^0\gamma^{\hat{+}}\tilde{T}(k_\perp)\right]\hat{M}^-\left[\tilde{T}(k_\perp - r_\perp)\gamma^{\hat{+}}\tilde{T}(p_\perp - r_\perp)\Lambda^+\gamma^0\right] = C(p_\perp, k_\perp, r_\perp)\hat{M}^-, \tag{71}$$

where

$$C(p_\perp, k_\perp, r_\perp) = \cos\left(\frac{\theta(p_\perp) - \theta(k_\perp)}{2}\right)\cos\left(\frac{\theta(r_\perp - p_\perp) - \theta(r_\perp - k_\perp)}{2}\right), \tag{72}$$

and

$$S(p_\perp, k_\perp, r_\perp) = \sin\left(\frac{\theta(p_\perp) - \theta(k_\perp)}{2}\right)\sin\left(\frac{\theta(r_\perp - p_\perp) - \theta(r_\perp - k_\perp)}{2}\right). \tag{73}$$

With Eqs. (68)-(71), we split Eq. (65) into the two coupled bound-state equations of $\hat{\phi}_+$ and $\hat{\phi}_-$

$$\left[-r_{\hat{+}} + E_u(p_\perp) - E_v(p_\perp - r_\perp)\right]\hat{\phi}_+(r_\perp, p_\perp) = \lambda \int \frac{\mathrm{d}k_\perp}{(p_\perp - k_\perp)^2}$$
$$\times \left[C(p_\perp, k_\perp, r_\perp)\hat{\phi}_+(r_\perp, k_\perp) - S(p_\perp, k_\perp, r_\perp)\hat{\phi}_-(r_\perp, k_\perp)\right], \tag{74a}$$

$$\left[r_{\hat{+}} + E_u(p_\perp - r_\perp) - E_v(p_\perp)\right]\hat{\phi}_-(r_\perp, p_\perp) = \lambda \int \frac{\mathrm{d}k_\perp}{(p_\perp - k_\perp)^2}$$
$$\times \left[C(p_\perp, k_\perp, r_\perp)\hat{\phi}_-(r_\perp, k_\perp) - S(p_\perp, k_\perp, r_\perp)\hat{\phi}_+(r_\perp, k_\perp)\right]. \tag{74b}$$

We again note here that Eqs. (74a)-(74b) coincide with Eq. (4.12) of Ref. [25] in the IFD as $\delta \to 0$ because not only the energies of particle and anti-particle become $E_u(p_\perp) \overset{\delta\to 0}{\longrightarrow} E(p^1)$ and $E_v(p_\perp) \overset{\delta\to 0}{\longrightarrow} -E(p^1)$ but also the rest of the variables correspond to their IFD counterparts, e.g. $r_{\hat{+}} \overset{\delta\to 0}{\longrightarrow} r^0$, etc..

In the LFD limit $\mathbb{C} \to 0$ (or $\delta \to \pi/4$) on the other hand, $E_u(p_\perp) \overset{\delta\to\pi/4}{\longrightarrow} B(p^+) + \frac{m^2}{2p^+} = \frac{m^2-2\lambda}{2p^+}$ and $E_v(p_\perp - r_\perp) \overset{\delta\to\pi/4}{\longrightarrow} -B(r^+ - p^+) - \frac{m^2}{2(r^+-p^+)} = -\frac{m^2-2\lambda}{2(r^+-p^+)}$ while $E_u(p_\perp - r_\perp) \overset{\delta\to\pi/4}{\longrightarrow} \frac{2(r^+-p^+)}{\mathbb{C}} + B(r^+ - p^+) + \frac{m^2}{2(r^+-p^+)}$ and $E_v(p_\perp) \overset{\delta\to\pi/4}{\longrightarrow} -\frac{2p^+}{\mathbb{C}}$ for the bound-state kinematics $0 < p^+ < r^+$. The bound-state kinematics $0 < p^+ < r^+$ in LFD automatically follows the dynamics given by Eqs. (74a) and (74b) in the limit $\delta \to \pi/4$ indicating the consistency with the positivity of the light-front longitudinal momenta. In this limit then, noting $C(p^+, k^+, r^+) \to 1$ and $S(p^+, k^+, r^+) \to 0$, we note that Eq. (74a) gets reduced to

$$\left[-r^- + \frac{m^2-2\lambda}{2p^+} + \frac{m^2-2\lambda}{2(r^+-p^+)}\right]\phi(r^+, p^+) = \lambda \int \frac{\mathrm{d}k^+}{(p^+-k^+)^2}\phi(r^+, k^+), \tag{75}$$

where $\phi(r^+, p^+)$ corresponds to $\hat{\phi}_+(r_\perp, p_\perp)$ in the LFD limit. Also, the solution for $\hat{\phi}_- \to 0$ can be attained rather immediately from Eq. (74b) by dividing it by the energy denominator factor $\left[r_{\hat{+}} + E_u(p_\perp - r_\perp) - E_v(p_\perp)\right]$ and noting the correspondence $1/(r_{\hat{+}} + E_u(p_\perp - r_\perp) - E_v(p_\perp)) \to \mathbb{C}/(2r^+ + \mathbb{C}(r^- + B(r^+ - p^+) + B(p^+) + \frac{m^2}{2(r^+-p^+)} + \frac{m^2}{2(p^+)}) \to 0$ as $\mathbb{C} \to 0$. Substituting the on-mass-shell condition $r^- = \mathcal{M}^2/(2r^+)$ for the bound-state meson of mass $\mathcal{M}$, defining the manifestly boost-invariant light-front momentum fraction variables $x = \frac{p^+}{r^+}(0 \le x \le 1)$ and $y = \frac{k^+}{r^+}(0 \le y \le 1)$ and multiplying both sides of the equation by $(-2r^+)$, we obtain

$$\left[\mathcal{M}^2 - \frac{m^2-2\lambda}{x} - \frac{m^2-2\lambda}{1-x}\right]\phi(x) = -2\lambda \int_0^1 \frac{dy}{(x-y)^2}\phi(y), \tag{76}$$

where the r^+ independence of $\phi(r^+, p^+)$ and $\phi(r^+, k^+)$ is imposed in $\phi(x)$ and $\phi(y)$ due to the boost-invariance of the light-front bound-state equation correctly reproducing 't Hooft's bound-state equation, Eq. (25) in Ref. [26]. We note that the above description of obtaining Eq. (76) is in essence equivalent to project the covariant Bethe-Salpeter amplitude into the light-front wavefunction defined at the equal light-front time.

In general, relating E_u's and E_v's in Eq. (74) to the solutions of E in Eq. (58), we summarize the interpolating coupled bound-state equations for $\hat{\phi}_+(r_\perp, p_\perp)$ and $\hat{\phi}_-(r_\perp, p_\perp)$ between IFD and LFD as follows:

$$\begin{aligned}
&\left[-r_{\hat{+}} + \frac{-\mathbb{S}p_\perp + E(p_\perp)}{\mathbb{C}} + \frac{\mathbb{S}(p_\perp - r_\perp) + E(p_\perp - r_\perp)}{\mathbb{C}}\right]\hat{\phi}_+(r_\perp, p_\perp) \\
&\quad = \lambda \int \frac{\mathrm{d}k_\perp}{(p_\perp - k_\perp)^2}\Big[C(p_\perp, k_\perp, r_\perp)\hat{\phi}_+(r_\perp, k_\perp) - S(p_\perp, k_\perp, r_\perp)\hat{\phi}_-(r_\perp, k_\perp)\Big], \qquad (77a) \\
&\left[r_{\hat{+}} + \frac{-\mathbb{S}(p_\perp - r_\perp) + E(p_\perp - r_\perp)}{\mathbb{C}} + \frac{\mathbb{S}p_\perp + E(p_\perp)}{\mathbb{C}}\right]\hat{\phi}_-(r_\perp, p_\perp) \\
&\quad = \lambda \int \frac{\mathrm{d}k_\perp}{(p_\perp - k_\perp)^2}\Big[C(p_\perp, k_\perp, r_\perp)\hat{\phi}_-(r_\perp, k_\perp) - S(p_\perp, k_\perp, r_\perp)\hat{\phi}_+(r_\perp, k_\perp)\Big]. \qquad (77b)
\end{aligned}$$

The reduction of these coupled equations to the light-front bound equation given by Eq. (76) may be displayed as Fig. 11. This reduction is remarkable as it provides a glimpse of the link between the light-front quark model (LFQM) and the first principle QCD.

The solutions of the bound-state equation may also be summarized by the meson spectroscopy depicted in Fig. 12 and the corresponding wavefunctions as presented in Ref. [14]. Fig. 12 depicts the feature of "Regge trajectories" for the quark-antiquark bound-states each with the corresponding equal bare mass m [26, 34, 38, 42, 43]. It is interesting to note that the Regge trajectory gets slightly modified from just the linear trajectory behavior, developing a bit of curvature in the trajectory for the ground-state and the low-lying excited states. For the small mass, in particular $m = 0$, the trajectory looks a little concave shape, while for the larger mass the curvature turns somewhat into a convex shape. This seems to reflect the fact that the GOR works in the chiral limit, but the chiral symmetry gets broken as the quark mass gets larger. The convex feature of the Regge trajectory for the heavy quarkonia model was shown in Ref. [44].

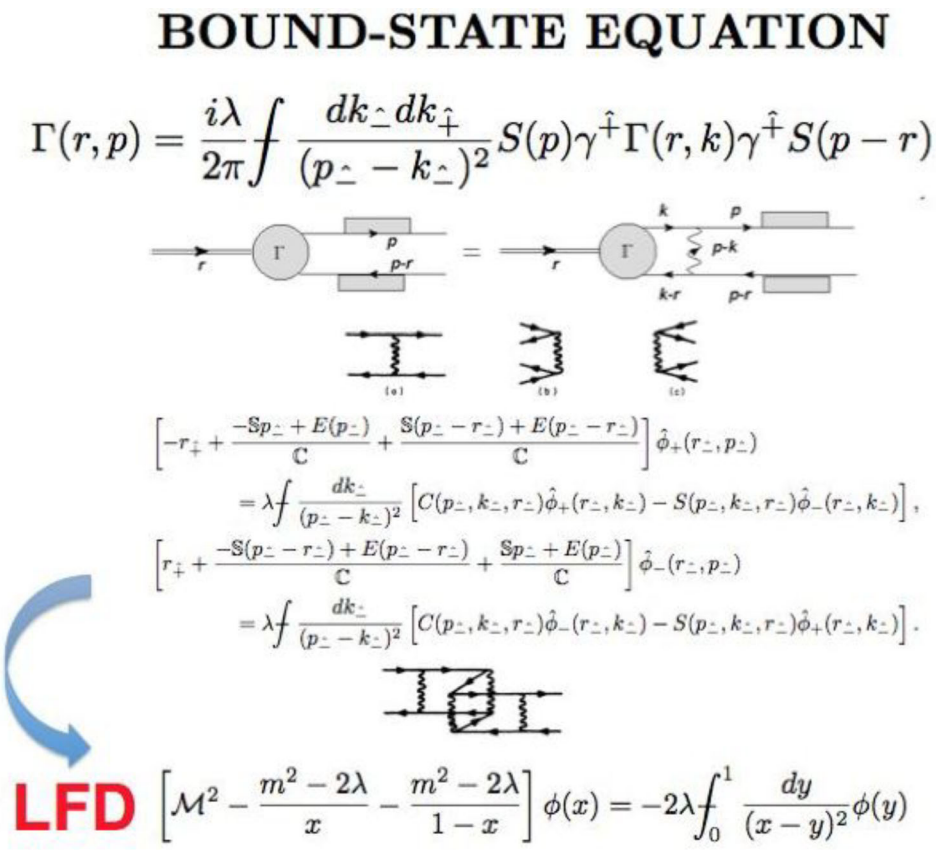

Fig. 11 Reduction of QCD coupled bound-state equations in LFD

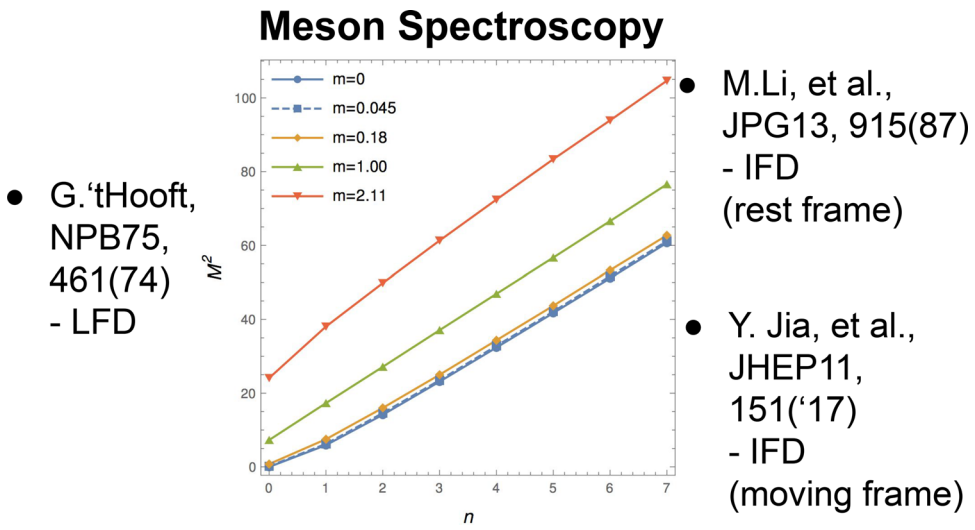

Fig. 12 Interpolation angle independence of meson spectroscopy

Since we obtained the bound-state wavefunctions, we applied them to compute the so-called quasi-PDFs which have been discussed extensively even in the 't Hooft model application [36] due to the possibility of computing directly the longitudinal momentum fraction x-dependence of the parton distributions in Euclidean lattice approach using the large momentum effective field theory (LaMET) program [45]. In our interpolating 't Hooft model computation, the "quasi-PDFs" may be defined as the following matrix element for the n-th state of the meson with the interpolating longitudinal momentum r^+:

$$\tilde{q}_{(n)}(r^+, x) = \int_{-\infty}^{+\infty} \frac{dx^-}{4\pi}\, e^{ix^- r^+} < r^+_{(n)}, r^+ \mid \bar{\psi}(x^-)\, \gamma^+\, \mathcal{W}[x^-, 0]\, \psi(0) \mid r^+_{(n)}, r^+ >_C, \tag{78}$$

where $r^{\hat{+}}_{(n)} = \sqrt{r^2_{\hat{-}} + \mathbb{C}\mathcal{M}^2_{(n)}}$ as the relationship for the energy-momentum of the on-mass-shell particle with mass m and two-momentum vector $p^{\hat{\mu}}$ is given by

$$(p^{\hat{+}})^2 = (p_{\hat{-}})^2 + \mathbb{C}m^2. \tag{79}$$

The range of the longitudinal momentum fraction $x = p_{\hat{-}}/r_{\hat{-}}$ is unconstrained, $-\infty < x < +\infty$, for $0 \le \delta < \pi/4$, while bounded, $0 \le x \le 1$, for $\delta = \pi/4$.

Interestingly, our numerical results of the interpolating "quasi-PDFs" in the moving frames indicate a possibility to utilize both variation of δ and $r_{\hat{-}}$ to attain the LFD result more effectively. Namely, one may not need to boost the longitudinal momentum $r_{\hat{-}}$ too large but search for a "sweet spot" by varying both δ and $r_{\hat{-}}$ together to obtain the "LFD-like" result. In IFD, $\delta = 0$ is fixed and thus the boost to the large longitudinal momentum is necessary for a successful approach to the LFD result. However, in the interpolating formulation between the IFD and the LFD, the LFD result can be approached even at rather small $r_{\hat{-}}$. Moreover, the application to the lattice formulation may be also possible with the existing technique of Wick rotation replacing the ordinary instant form time x^0 by the interpolating time $x^{\hat{+}}$ in the process of taking the "imaginary time" in the lattice as far as δ remains in the region $0 \le \delta < \pi/4$ avoiding the light-like surface $\delta = \pi/4$. As discussed in Ref. [14], one can match the Minkowski space and the Euclidean space confirming the correspondence given by

$$p'^2_{\hat{-}} \leftrightarrow -\tilde{P}^2, \tag{80}$$

where the square of the rescaled longitudinal momentum $(p'_{\hat{-}})$ corresponds to the Euclidean variable $\tilde{P}^2$ for the space-like region $\tilde{P}^2 < 0$ in the interpolating dynamics. For an illustration of the δ variation for a given finite $r_{\hat{-}}$, we take rather small momentum of the meson for the case of $m = 0$ and show the "quasi-PDFs" of the ground-state for the variation of δ parameter as $\delta = 0$, $\delta = 0.6$ and $\delta = 0.78$ in Fig. 13. The notation $\mathbf{M}_{0.18} = 0.88$ used in Fig 13 denotes the ground-state meson mass for $m = 0.18$ in the proper unit of $\sqrt{2\lambda}$ as the reference value of the interpolating longitudinal momentum $r_{\hat{-}}$. The details of the numerical computation can be found in Ref. [14]. It indicates that a pretty slow approach to the LFD result in the large-momentum IFD can be fairly well expedited by taking δ away from the IFD ($\delta = 0$) and getting closer to the LFD ($\delta = \pi/4$) while the same value of the longitudinal momentum $r_{\hat{-}} = 2\mathbf{M}_{0.18}$ is taken. We think it would be worthwhile to explore this idea of utilizing the interpolating formulation between IFD and LFD for the application to the lattice computation.

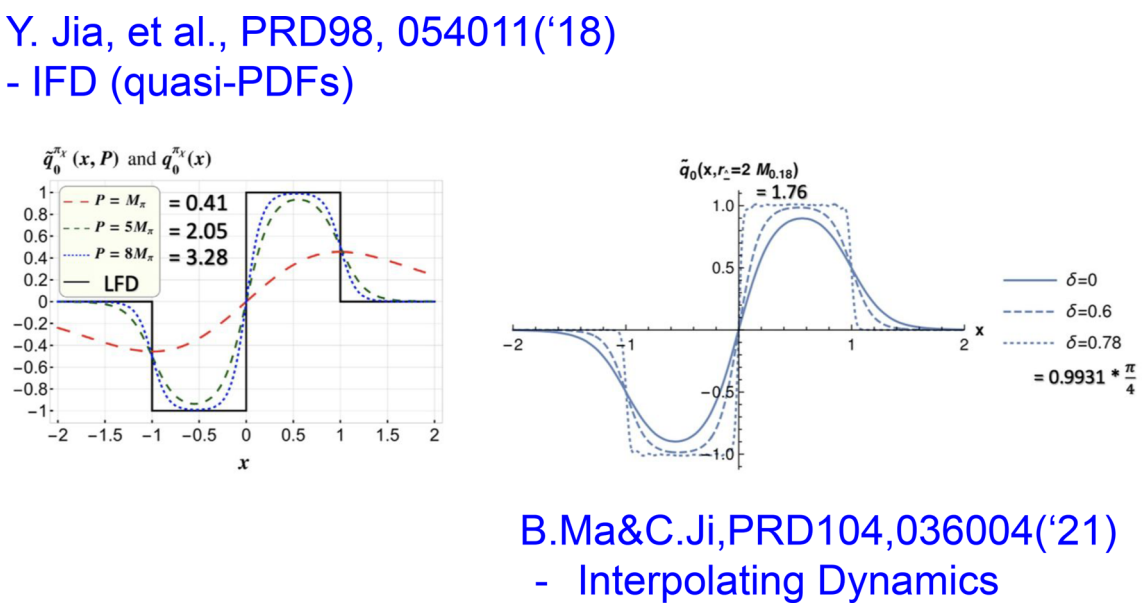

Fig. 13 Quasi-PDFs in IFD vs. Interpolating quasi-PDFs

4 Conclusion and outlook

In this review, we discussed the fundamental aspects of the time-ordered scattering amplitudes in relativistic Hamiltonian dynamics. Using the interpolating angle between IFD and LFD, we presented a simple but clear example of interpolating scattering amplitudes and demonstrated a physical meaning of kinematical transformations introduced often formally in the stability group of Poincaré transformations. We confirmed the well-known IMF result [17] for the IFD and extended it for any arbitrary interpolating angle $0 \leq \delta < \frac{\pi}{4}$. We also showed that the disappearance of the connected contributions to the current from the vacuum in LFD is independent of the reference frame and should be distinguished from the IMF result. This demonstrates that the longitudinal boost K^3 becomes kinematical and joins the stability group only in the LFD. This distinguished property of the longitudinal boost K^3 could be shown explicitly using the expressions of kinematic transformation effects on the fundamental dynamical variables of physical momenta, while we discussed this property of K^3 using the interpolating time-ordered scattering amplitudes. The addition of K^3 in the stability group is a great advantage of LFD in hadron phenomenology [46].

We have also completed the interpolation of Quantum Electrodynamics between the instant form and the front form proposed by Dirac [1]. We started from the QED Lagrangian and presented the interpolating Hamiltonian formulation introducing a parameter δ which corresponds between the IFD at $\delta = 0$ and the front-form dynamics which we call the LFD at $\delta = \pi/4$. Not only have we summarized the interpolating time-ordered diagram rules for the computation of QED processes in terms of the interpolation angle parameter $0 \leq \delta \leq \pi/4$, but also we have applied these rules to the typical QED processes such as $e^+e^- \to \gamma\gamma$ and $e\gamma \to e\gamma$ which involve the fermion propagator beyond what we have already presented in our previous works [11, 12]. Entwining the fermion propagator interpolation with our previous works of the interpolating helicity spinors and the electromagnetic gauge field interpolation, we have now fastened the bolts and nuts necessary in launching the interpolating QED.

In this review, we also discussed the interpolation of the 't Hooft model (i.e. QCD_2 in the large N_c limit) with the interpolation angle δ between IFD ($\delta = 0$) and LFD ($\delta = \pi/4$) and presented its nontrivial vacuum effects on the quark mass and wavefunction renormalization as well as the corresponding meson mass and wavefunction properties taking the meson as the quark-antiquark bound-state. We derived the interpolating the mass gap equation between IFD and LFD using not only the algebraic method based on the Bogoliubov transformation between the trivial and nontrivial vacuum as well as the bare and dressed quark but also the diagrammatic method based on the self-consistent embodiment of the quark self-energy [14]. Our mass gap solutions agree not only with the LFD result in Ref. [26] for $\delta = \pi/4$ but also with the IFD results in Refs. [42, 43] for $\delta = 0$. The renormalized chiral condensate was computed and the agreement of the result in the chiral limit was verified with the exact result in Ref. [29, 30]. Its invariance regardless of the δ values between IFD and LFD was also confirmed. Taking into account the wavefunction renormalization factor $F(p_{\hat{-}})$ as well as the mass function $M(p_{\hat{-}})$ and expressing the dressed quark propagator $S(p)$ in terms of $F(p_{\hat{-}})$ and $M(p_{\hat{-}})$ as given by Eq. (46), we resolved the issue of $E(p_{\hat{-}})$ not being always positive for $m \lesssim 0.56$ discussed in Ref. [25]. Extending the interpolating energy-momentum dispersion relation of the on-mass-shell particle given by Eq. (79) to the case of the dressed quark with the rescaled variable given by Eq. (54), we obtained the interpolation angle independent energy function $\tilde{E}(p'_{\hat{-}})$. Typical profiles of $\tilde{E}(p'_{\hat{-}})$ were exemplified in Fig. 9.

Utilizing the dressed fermion propagators, we then derived the quark-antiquark bound-state equation interpolating between IFD and LFD for the equal bare quark and antiquark mass m and solved numerically the corresponding bound-state equations. The reduction of the coupled equations to the light-front bound equation displayed in Fig. 11 is remarkable as it provides a glimpse of the link between the light-front quark model (LFQM) and the first principle QCD.

From the numerical solutions of the spectroscopy, we find that the meson mass spectrum is independent of the interpolation angle between the IFD and LFD as expected for physical observables. Applying the bound-state wavefunctions $\hat{\phi}^{(n)}_{\pm}(r_{\hat{-}}, x)$ for the computation of the interpolating "quasi-PDFs" given by Eq. (78), we note the consistency with the observation made in Ref. [36] for the quasi-PDFs at $\delta = 0$ (IFD) that there exists considerable difference between the shapes of the LFD result and the IFD quasi-PDF result for the light mesons. Our results indicate that the slow approach to the LFD-like results may be remedied by varying the interpolation parameter δ as well as the interpolating longitudinal meson momentum $r_{\hat{-}}$. For the future work, one may explore such an idea to search for the "sweet spot" of δ and $r_{\hat{-}}$ to attain most effective computation with the least sensitive numerical errors in getting the LFD result. Extending the Wick rotation technique to the interpolating time $x^{\hat{+}}$, the idea of searching for the "sweet spot" may be applicable to the usual lattice formulation in the Euclidean space. This would be in good contrast to the recent application of the present interpolating formulation to the two-dimensional ϕ^4 theory using the discretization technique in Minkowski space consistent with the discrete light-cone quantization (DLCQ) approach [47, 48]. It will be interesting to explore both "Euclidean" and "Minkowski" numerical approaches implementing the interpolating formulation between IFD and LFD.

Acknowledgements This work was supported in part by the U.S. Department of Energy(Grant No. DE-FG02-03ER41260). The National Energy Research Scientific Computing Center (NERSC) supported by the Office of Science of the U.S. Department of Energy under Contract No. DE-AC02-05CH11231 is also acknowledged. The author acknowledges all the co-authors of the papers collaborated with the author cited in this review article and the hospitality during his visit to APCTP where this paper was completed.

Data Availability No Data associated in the manuscript

References

1. P. Dirac, Forms of relativistic dynamics. Rev. Mod. Phys. **21**, 392–399 (1949). https://doi.org/10.1103/RevModPhys.21.392
2. S. Fubini, A.J. Hanson, R. Jackiw, New approach to field theory. Phys. Rev. D **7**, 1732–1760 (1973). https://doi.org/10.1103/PhysRevD.7.1732
3. L.Y. Glozman, W. Plessas, K. Varga, R.F. Wagenbrunn, Unified description of light- and strange-baryon spectra. Phys. Rev. D **58**, 094030 (1998). https://doi.org/10.1103/PhysRevD.58.094030
4. R.F. Wagenbrunn, S. Boffi, W. Klink, W. Plessas, M. Radici, Covariant nucleon electromagnetic form-factors from the Goldstone boson exchange quark model. Phys. Lett. B **511**, 33–39 (2001). https://doi.org/10.1016/S0370-2693(01)00622-0. arXiv:nucl-th/0010048
5. T. Melde, K. Berger, L. Canton, W. Plessas, R.F. Wagenbrunn, Electromagnetic nucleon form factors in instant and point form. Phys. Rev. D **76**, 074020 (2007). https://doi.org/10.1103/PhysRevD.76.074020
6. C.-R. Ji, *Relativistic Quantum Invariance: Lecture Notes in Physics*, vol. 1012 (Springer, Singapore, 2023)
7. E.V. Prokhvatilov, V.A. Franke, Limiting transition to lightlike coordinates in the field theory and qcd Hamiltonian. Sov. J. Nucl. Phys. **49**, 688–692 (1989). (**in Russian**)
8. F. Lenz, M. Thies, K. Yazaki, S. Levit, Hamiltonian formulation of two-dimensional gauge theories on the light cone. Ann. Phys. **208**, 1–89 (1991). https://doi.org/10.1016/0003-4916(91)90342-6
9. H. Naus, H.J. Pirner, T.J. Fields, J.P. Vary, Qcd near the light cone. Phys. Rev. D **56**, 8062–8073 (1997). https://doi.org/10.1103/PhysRevD.56.8062
10. C.-R. Ji, A.T. Suzuki, Interpolating scattering amplitudes between the instant form and the front form of relativistic dynamics. Phys. Rev. D **87**, 065015 (2013). https://doi.org/10.1103/PhysRevD.87.065015
11. C.-R. Ji, Z. Li, A.T. Suzuki, Electromagnetic gauge field interpolation between the instant form and the front form of the Hamiltonian dynamics. Phys. Rev. D **91**, 065020 (2015). https://doi.org/10.1103/PhysRevD.91.065020
12. Z. Li, M. An, C.-R. Ji, Interpolating helicity spinors between the instant form and the light-front form. Phys. Rev. D **92**, 105014 (2015). https://doi.org/10.1103/PhysRevD.92.105014
13. C.-R. Ji, Z. Li, B. Ma, A.T. Suzuki, Interpolating quantum electrodynamics between instant and front forms. Phys. Rev. D **98**, 036017 (2018). https://doi.org/10.1103/PhysRevD.98.036017
14. B. Ma, C.-R. Ji, Interpolating 't Hooft model between instant and front forms. Phys. Rev. D **104**, 036004 (2021). https://doi.org/10.1103/PhysRevD.104.036004
15. K. Hornbostel, Nontrivial Vacua from equal time to the light cone. Phys. Rev. D **45**, 3781–3801 (1992). https://doi.org/10.1103/PhysRevD.45.3781
16. C.-R. Ji, C. Mitchell, Poincaré invariant algebra from instant to light-front quantization. Phys. Rev. D **64**, 085013 (2001). https://doi.org/10.1103/PhysRevD.64.085013
17. S. Weinberg, Dynamics at infinite momentum. Phys. Rev. **150**, 1313–1318 (1966). https://doi.org/10.1103/PhysRev.150.1313
18. R.J. Perry, A. Harindranath, K.G. Wilson, Light-front Tamm-Dancoff field theory. Phys. Rev. Lett. **65**, 2959–2962 (1990). https://doi.org/10.1103/PhysRevLett.65.2959
19. G. Leibbrandt, Light-cone gauge in yang-mills theory. Phys. Rev. D **29**, 1699–1708 (1984). https://doi.org/10.1103/PhysRevD.29.1699
20. P.P. Srivastava, S.J. Brodsky, Light-front-quantized qcd in the light-cone gauge: The doubly transverse gauge propagator. Phys. Rev. D **64**, 045006 (2001). https://doi.org/10.1103/PhysRevD.64.045006
21. A.T. Suzuki, J. Sales, Light front gauge propagator reexamined. Nucl. Phys. A **725**, 139–148 (2003). https://doi.org/10.1016/S0375-9474(03)01575-6. arXiv:nucl-th/0303016
22. L. Mantovani, B. Pasquini, X. Xiong, A. Bacchetta, Revisiting the equivalence of light-front and covariant qed in the light-cone gauge. Phys. Rev. D **94**, 116005 (2016). https://doi.org/10.1103/PhysRevD.94.116005

23. S.-J. Chang, T.-M. Yan, Quantum field theories in the infinite-momentum frame. ii. scattering matrices of scalar and dirac fields. Phys. Rev. D **7**, 1147–1161 (1973). https://doi.org/10.1103/PhysRevD.7.1147
24. J.B. Kogut, D.E. Soper, Quantum electrodynamics in the infinite-momentum frame. Phys. Rev. D **1**, 2901–2914 (1970). https://doi.org/10.1103/PhysRevD.1.2901
25. I. Bars, M.B. Green, Poincaré- and gauge-invariant two-dimensional quantum chromodynamics. Phys. Rev. D **17**, 537–545 (1978). https://doi.org/10.1103/PhysRevD.17.537
26. G. Hooft, A two-dimensional model for mesons. Nucl. Phys. B **75**, 461–470 (1974). https://doi.org/10.1016/0550-3213(74)90088-1
27. G. Hooft, A planar diagram theory for strong interactions. Nucl. Phys. B **72**, 461 (1974). https://doi.org/10.1016/0550-3213(74)90154-0
28. E. Witten, Baryons in the 1/n expansion. Nucl. Phys. B **160**, 57–115 (1979). https://doi.org/10.1016/0550-3213(79)90232-3
29. A.R. Zhitnitsky, On chiral symmetry breaking in QCD in two-dimensions ($N_c \to$ Infinity). Phys. Lett. B **165**, 405–409 (1985). https://doi.org/10.1016/0370-2693(85)91255-9
30. A.R. Zhitnitsky, State spectrum, low-energy theorems and sum rules in QCD in two-dimensions (N(c) $\to$ Infinity). Sov. J. Nucl. Phys. **44**, 139–144 (1986). (**in Russian**)
31. V. Baluni, The Bose form of two-dimensional quantum chromodynamics. Phys. Lett. B **90**, 407–412 (1980). https://doi.org/10.1016/0370-2693(80)90960-0
32. G. Bhattacharya, Equivalence between two-dimensional SU(n) QCD and Schwinger model: an analysis of strong coupling phase. Nucl. Phys. B **205**, 461–482 (1982). https://doi.org/10.1016/0550-3213(82)90370-4
33. P.J. Steinhardt, Baryons and Baryonium in QCD in two-dimensions. Nucl. Phys. B **176**, 100–112 (1980). https://doi.org/10.1016/0550-3213(80)90065-6
34. C.G. Callan, N. Coote, D.J. Gross, Two-dimensional yang-mills theory: a model of quark confinement. Phys. Rev. D **13**, 1649–1669 (1976). https://doi.org/10.1103/PhysRevD.13.1649
35. Y. Frishman, C.T. Sachrajda, H. Abarbanel, R. Blankenbecler, Novel inconsistency in two-dimensional gauge theories. Phys. Rev. D **15**, 2275–2281 (1977). https://doi.org/10.1103/PhysRevD.15.2275
36. Y. Jia, S. Liang, X. Xiong, R. Yu, Partonic quasidistributions in two-dimensional qcd. Phys. Rev. D **98**, 054011 (2018). https://doi.org/10.1103/PhysRevD.98.054011
37. C.-R. Ji, Pion loops in chiral perturbation theory and light-front dynamics. Few Body Syst. **52**, 421–426 (2012). https://doi.org/10.1007/s00601-011-0270-5
38. R.C. Brower, W.L. Spence, J.H. Weis, Bound states and asymptotic limits for quantum chromodynamics in two dimensions. Phys. Rev. D **19**, 3024–3049 (1979). https://doi.org/10.1103/PhysRevD.19.3024
39. B. Grinstein, R.F. Lebed, Explicit quark-hadron duality in heavy-light meson weak decays in the 't Hooft model. Phys. Rev. D **57**, 1366–1378 (1998). https://doi.org/10.1103/PhysRevD.57.1366
40. M. Burkardt, N. Uraltsev, Analytical heavy quark expansion in the 't Hooft model. Phys. Rev. D **63**, 014004 (2000). https://doi.org/10.1103/PhysRevD.63.014004
41. L.Y. Glozman, V.K. Sazonov, M. Shifman, R.F. Wagenbrunn, How chiral symmetry breaking affects the spectrum of the light-heavy mesons in the 't Hooft model. Phys. Rev. D **85**, 094030 (2012). https://doi.org/10.1103/PhysRevD.85.094030
42. M. Li, L. Wilets, M.C. Birse, QCD in two-dimensions in the axial gauge. J. Phys. G **13**, 915–923 (1987). https://doi.org/10.1088/0305-4616/13/7/005
43. Y. Jia, S. Liang, L. Li, X. Xiong, Solving the Bars-Green equation for moving mesons in two-dimensional QCD. JHEP **11**, 151 (2017). https://doi.org/10.1007/JHEP11(2017)151. arXiv:1708.09379 [hep-ph]
44. M.M. Brisudová, L. Burakovsky, T. Goldman, Effective functional form of Regge trajectories. Phys. Rev. D **61**, 054013 (2000). https://doi.org/10.1103/PhysRevD.61.054013
45. X. Ji, Parton physics on a Euclidean lattice. Phys. Rev. Lett. **110**, 262002 (2013). https://doi.org/10.1103/PhysRevLett.110.262002
46. C.E. Carlson, C.-R. Ji, Angular conditions, relations between the Breit and light-front frames, and subleading power corrections. Phys. Rev. D **67**, 116002 (2003). https://doi.org/10.1103/PhysRevD.67.116002
47. S.S. Chabysheva, J.R. Hiller, Transitioning from equal-time to light-front quantization in ϕ_2^4 theory. Phys. Rev. D **102**, 116010 (2020). https://doi.org/10.1103/PhysRevD.102.116010
48. Hornbostel, K.: The application of light cone quantization to quantum chromodynamics in (1+1)-dimensions. Phd thesis (1988)